Differential contribution of two organelles of endosymbiotic origin to iron-sulfur cluster synthesis and overall fitness in Toxoplasma

Sarah Pamukcu[1], Aude Cerutti[1], Yann Bordat[1], Sonia Hem[2], Valérie Rofidal[2], Sébastien Besteiro[3*]

[1]LPHI, Univ Montpellier, CNRS, Montpellier, France

[2]BPMP, Univ Montpellier, CNRS, INRAE, Institut Agro, Montpellier, France

[3]LPHI, Univ Montpellier, CNRS, INSERM, Montpellier, France

* sebastien.besteiro@inserm.fr

Abstract

Iron-sulfur (Fe-S) clusters are one of the most ancient and ubiquitous prosthetic groups, and they are required by a variety of proteins involved in important metabolic processes. Apicomplexan parasites have inherited different plastidic and mitochondrial Fe-S clusters biosynthesis pathways through endosymbiosis. We have investigated the relative contributions of these pathways to the fitness of *Toxoplasma gondii*, an apicomplexan parasite causing disease in humans, by generating specific mutants. Phenotypic analysis and quantitative proteomics allowed us to highlight notable differences in these mutants. Both Fe-S cluster synthesis pathways are necessary for optimal parasite growth in vitro, but their disruption leads to markedly different fates: impairment of the plastidic pathway leads to a loss of the organelle and to parasite death, while disruption of the mitochondrial pathway trigger differentiation into a stress resistance stage. This highlights that otherwise similar biochemical pathways hosted by different sub-cellular compartments can have very different contributions to the biology of the parasites, which is something to consider when exploring novel strategies for therapeutic intervention.

Author summary

Toxoplasma gondii is a ubiquitous unicellular parasite that harbours two organelles of endosymbiotic origin: the mitochondrion, and a relict plastid named the apicoplast. Each one of these organelles contains its own machinery for synthesizing iron-sulfur clusters, which are important protein co-factors. In this study, we show that interfering with either the mitochondrial or the plastidic iron-sulfur cluster synthesizing machinery has a profound impact on parasite growth. However, while disrupting the plastidic pathway led to an irreversible loss of the organelle and subsequent death of the parasite, disrupting the mitochondrial pathway led to conversion of the parasites into a stress resistance form. We used a comparative quantitative proteomic analysis of the mutants, combined with experimental validation, to provide mechanistic clues into these different phenotypic outcomes. Although the consequences of disrupting each pathway were manifold, our data highlighted distinct changes at the metabolic level. For instance, the plastidic iron-sulfur cluster synthesis pathway is likely important for maintaining the lipid homeostasis of the parasites, while the mitochondrial pathway is clearly crucial for maintaining their respiratory capacity. Interestingly, we have discovered that other mutants severely impacted for mitochondrial function, in particular the respiratory chain, are able to survive and initiate conversion to the stress resistance form. This illustrates a different capacity for *T. gondii* to adapt for survival in response to distinct metabolic dysregulations.

Keywords: iron-sulfur cluster, Toxoplasma, differentiation, bradyzoite, apicoplast, mitochondrion

Short title: Iron-sulfur cluster synthesis in *Toxoplasma*

Introduction

Endosymbiotic events were crucial in the evolutionary timeline of eukaryotic cells. Mitochondria and plastids evolved from free-living prokaryotes that were taken up by early eukaryotic ancestors and transformed into permanent subcellular compartments that have become essential for harnessing energy or synthesizing essential metabolites in present-day eukaryotes [1]. As semiautonomous organelles, they contain a small genome, but during the course of evolution a considerable part of their genes have been transferred to the cell nucleus. Yet, they rely largely on nuclear factors for their maintenance and expression. Both organelles are involved in critically important biochemical processes. Mitochondria, which are found in most eukaryotic organisms, are mostly known as the powerhouses of the cell, owing to their ability to produce ATP through respiration. Importantly, they are also involved in several other metabolic pathways [2], including the synthesis of heme groups, steroids, amino acids, and iron-sulfur (Fe-S) clusters. Moreover, they have important cellular functions in regulating redox and calcium homeostasis. Similarly, plastids that are found in plants, algae and some other eukaryotic organisms, host a diverse array of pathways that contribute greatly to the cellular metabolism [3]. While often identified mainly as compartments where photosynthesis occurs, plastids host other important metabolic pathways. For example, they are involved in the assimilation of nitrogen and sulfur, as well as the synthesis of carbohydrates, amino acids, fatty acids and specific lipids, hormone precursors, and also Fe-S clusters. The best-characterized plastid is arguably the plant cell chloroplast, but not all plastids have photosynthetic function, and in higher plants they are in fact a diverse group of organelles that share basal metabolic pathways, but also have specific physiological roles [4].

The phylum Apicomplexa comprises a large number of single-celled protozoan parasites responsible for serious disease in animals, including humans. For example, this phylum includes parasites of the genus *Plasmodium* that are responsible for the deadly malaria, and *Toxoplasma gondii* a ubiquitous parasite that can lead to a severe pathology in immunocompromised individuals. Apicomplexan parasites evolved from a photosynthetic ancestor and many of them still retain a plastid [5,6]. This plastid, named the apicoplast, originated from a secondary endosymbiotic event [7,8]. It has lost its photosynthetic properties as the ancestors of Apicomplexa switched to an intracellular parasitic lifestyle [9]. The apicoplast nevertheless still hosts four main metabolic pathways [10,11]: a so-called non-mevalonate pathway for the synthesis of isoprenoid precursors, a type II fatty acid synthesis pathway (FASII), part of the heme synthesis pathway, and a Fe-S cluster synthesis pathway. As the apicoplast is involved in these important biological processes for the parasite, and as they markedly differ from those of the host (because of their algal origin), that makes it a valuable potential drug target. Apicomplexan parasites also generally contain a single tubular mitochondrion, although its aspect may vary during parasite development [12,13]. The organelle is an important contributor to the parasite's metabolic needs [14]. It classically hosts tricarboxylic acid (TCA) cycle reactions, which are the main source of electrons that feeds the mitochondrial electron transport chain (ETC) which generates a proton gradient used for ATP production. It also contains additional metabolic pathways, like a Fe-S cluster synthesis pathway and part of the heme synthesis pathway operating in collaboration with the apicoplast. The latter reflects obvious functional links between the organelles and potential metabolic interactions, which is also illustrated by their physical connection during parasite development [15,16].

Fe-S clusters are simple and ubiquitous cofactors involved in a great variety of cellular processes. As their name implies, they are composed of iron and inorganic sulfur whose chemical properties confer key structural or electron transfer features to proteins in all kingdoms of life. They are important to the activities of numerous proteins that play essential roles to sustain fundamental life processes

including, in addition to electron transfer and exchange, iron storage, protein folding, oxygen/nitrogen stress sensing, and gene regulation [17]. The synthesis of Fe-S clusters and their insertion into apoproteins requires complex machineries and several distinct pathways have been identified in bacteria for synthesizing these ancient cofactors [18]. They include the ISC (iron-sulfur cluster) pathway for general Fe–S cluster assembly [19], and the SUF (sulfur formation) pathway [20] that is potentially activated in oxidative stress conditions [21]. Eukaryotes have inherited machineries for synthesizing Fe-S cluster through their endosymbionts [22]. As a result, organisms with both mitochondria and plastids, like land plants, use the ISC pathway for assembling Fe-S clusters in the mitochondria and the SUF pathway for Fe-S clusters in the plastids [23]. Additional protein components that constitute a cytosolic Fe-S cluster assembly machinery (CIA) have also been identified: this pathway is important for the generation of cytosolic, but also of nuclear Fe-S proteins, and is highly dependent on the ISC mitochondrial pathway for providing a sulfur-containing precursor [24].

Like in plants and algae, apicoplast-containing Apicomplexa seem to harbour the three (ISC, SUF and CIA) Fe-S cluster synthesis pathways. Although the CIA pathway was recently shown to be important for *Toxoplasma* fitness [25], investigations in apicomplexan parasites have been so far almost exclusively focused on the apicoplast-located SUF pathway [26–30] and mostly in *Plasmodium* species. The SUF pathway was shown to be essential for the viability of malaria parasites during both the erythrocytic and sexual stages of development, and has thus been recognized as a putative avenue for discovering new antiparasitic drug targets (reviewed in [31]). Contrarily to the ISC pathway, which is also present in the mammalian hosts of apicomplexan parasites, the SUF pathway may indeed yield interesting specificities that may be leveraged for therapeutic intervention. However, very little is known about Fe-S clusters synthesis in other apicomplexan parasites, including *T. gondii*. For instance, out of the four known metabolic pathways hosted by the apicoplast, Fe-S synthesis was the only one remaining to be functionally investigated in *T. gondii*, while the others were all shown to be essential for the tachyzoite stage of the parasite (a fast replicating developmental stage responsible for the symptoms of the disease) [32–35]. Here, we present the characterization of two *T. gondii* mutants we generated to specifically impact the plastidic and mitochondrial SUF and ISC pathways, respectively. Our goal was to assess the relative contributions of these compartmentalized pathways to parasite development and fitness.

Results

TgNFS2 and TgISU1 are functional homologs of components of the Fe-S cluster synthesis pathways

Fe-S cluster biosynthesis pathways in the mitochondrion and the plastid follow a similar general pattern: cysteine desulfurases (NFS1, NFS2) produce sulfur from L-cysteine, scaffold proteins (ISU1, SufB/C/D) provide a molecular platform allowing iron and sulfur to meet and form a cluster, and finally carrier proteins (like IscA or SufA) deliver the cluster to target apoproteins [23]. The cytosolic CIA pathway, which is responsible for the de novo formation of Fe-S clusters to be incorporated in cytosolic and nuclear proteins, is dependent on the ISC pathway, as its first step requires the import of a yet unknown sulfur-containing precursor that is translocated to the cytosol from the mitochondrion [24]. To get a general overview of the predicted components for the Fe-S cluster machinery in *T. gondii*, we conducted homology searches in the ToxoDB.org database [36], using well-characterized proteins from plants (*Arabidopsis thaliana*) belonging to the SUF, ISC and CIA pathways (Table S1). Data from global mapping of protein subcellular location by hyperLOPIT spatial proteomics [37] was in general in good accordance with the expected localization of the homologs

137 (with the noticeable exception of members of the NBP35/HCF101 ATP-binding proteins). Overall, our
138 search revealed that *T. gondii* appeared to have a good conservation of all the main components of
139 the three ISC, SUF and CIA Fe-S synthesis pathways (Table S1, Figure 1A). Additional information
140 available on ToxoDB.org such as scores from a CRISPR/Cas9-based genome-wide screening [38],
141 highlighted that most components of the three pathways are predicted to be important for parasite
142 fitness. This suggests several Fe-S proteins localizing to the endosymbiotic organelles, but also the
143 cytosol/nucleus, are essential for the optimal growth of tachyzoites. In order to verify this, our aim
144 was to specifically interfere with the apicoplast-localized SUF pathway or the mitochondrion-
145 localized ISC pathway in *T. gondii* tachyzoites. More precisely, we wanted to target the homologs of
146 *A. thaliana* NFS2 and ISU1, which are both central (and presumably essential) to their respective
147 pathways (Figure 1A): NFS2 is a cysteine desulfurase that provides the inorganic sulfur part of
148 plastidic Fe-S clusters, while ISU1 is a scaffold protein important for cluster assembly in the
149 mitochondrial pathway. Interfering with these key players of the upstream machinery would likely
150 lead to a comparable disruption of the respective Fe-S cluster biogenesis pathways hosted by each
151 organelle [39].

152 As a first step, we sought to determine whether TgNFS2 (TGGT1_216170) and TgISU1
153 (TGGT1_237560) were real functional homologs by performing complementation assays of bacterial
154 mutants. In many bacteria, the ISC machinery is the primary system for general Fe-S cluster
155 biosynthesis, while the SUF system plays a similar general role, but is mostly operative under stress
156 conditions (like iron limitation or oxidative stress). In *Escherichia coli*, both pathways are partially
157 redundant, but their individual disruption results in slowed bacterial growth, especially when limiting
158 iron availability with a specific chelator [40]. Expression of the predicted functional domains of
159 TgNFS2 and TgISU1 in mutant strains for the corresponding *E. coli* proteins (named SUFS and ISCU,
160 respectively) improved bacterial growth, in the presence of an iron chelator or not (Figure 1B). The
161 complementation seemed partial as complemented strains remained more sensitive to the iron
162 chelator than the wild-type strain. Yet, and although stationary phase was reached earlier than for
163 the wild-type bacteria, contrarily to the mutants the complemented strains showed a bacterial
164 density close to that of the WT at stationary phase. This suggests TgNFS2 and TgISU1, in addition to a
165 good sequence homology with their bacterial homologues (Figure S1), have a conserved function.

166 We next determined the sub-cellular localizations of TgNFS2 and TgISU1 by epitope tagging of the
167 native proteins. This was achieved in the TATi ΔKu80 cell line, which favors homologous
168 recombination and would allow transactivation of a Tet operator-modified promoter we would later
169 use for generating a conditional mutant in this background [41–43]. A sequence coding for a C-
170 terminal triple hemagglutinin (HA) epitope tag was inserted at the endogenous *TgNFS2* or *TgISU1*
171 locus by homologous recombination (Figure S2). Using the anti-HA antibody, by immunoblot we
172 detected two products for each protein (Figure 2A, B), likely corresponding to their immature and
173 mature forms (ie after cleavage of the transit peptide upon import into the organelle). Accordingly,
174 the analysis of TgNFS2 and TgISU1 sequences with several subcellular localization and N-terminal
175 sorting signals site predictors confirmed they likely contained sequences for plastidic and
176 mitochondrial targeting [44], respectively, although no consensus position of the exact cleavage sites
177 could be determined. Immunofluorescence assay (IFA) in *T. gondii* tachyzoites confirmed HA-tagged
178 TgNFS2 and TgISU1 co-localize with markers of the apicoplast and the mitochondrion, respectively
179 (Figure 2C, D).

180 NFS2 is a cysteine desulfurase whose activity is enhanced by an interaction with the SUFE protein
181 [45]. Similar to plants that express several SUFE homologues [46], there are two putative SUFE-like
182 proteins in *T. gondii* (Table S1), one of which was already predicted to reside in the apicoplast by

183 hyperLOPIT (TgSUFE1, TGGT1_239320). We generated a cell line expressing an HA-tagged version of
184 the other, TgSUFE2 (TGGT1_277010, Figure S3A, B, C), whose localization was previously unknown.
185 Like for TgNFS2, several programs predicted a plastidic transit peptide, which was confirmed by
186 immunoblot analysis (detecting TgSUFE2 immature and mature forms, Figure S3D). IFA showed
187 TgSUFE2 co-localizes with an apicoplast marker (Figure S3E). This further confirms that the initial
188 steps of Fe-S cluster biogenesis in the apicoplast are likely functionally-conserved.

189

190 **Disruption of either the plastidic or the mitochondrial Fe-S cluster pathway has a profound impact**
191 **on parasite growth**

192 In order to get insights into plastidic and mitochondrial Fe-S biogenesis, we generated conditional
193 mutant cell lines in the TgNFS2-HA or TgISU1-HA-expressing TATi ΔKu80 background [43].
194 Replacement of the endogenous promoters by an inducible-Tet07*SAG4* promoter, through a single
195 homologous recombination at the loci of interest (Figure S4), yielded TgNFS2 and TgISU1 conditional
196 knock-down cell lines (cKD TgNFS2-HA and cKD TgISU1-HA, respectively). In these cell lines, the
197 addition of anhydrotetracycline (ATc) can repress transcription through a Tet-Off system [47]. For
198 each cKD cell line several transgenic clones were obtained and were found to behave similarly in the
199 initial phenotypic assays we performed, so only one was analysed further. Transgenic parasites were
200 grown for various periods of time in presence of ATc, and protein down-regulation was evaluated.
201 Immunoblot and IFA analyses of cKD further -HA and cKD TgISU1-HA parasites showed that the
202 addition of ATc efficiently down-regulated the expression of *TgNFS2* (Figure 3A, C) and *TgISU1*
203 (Figure 3B, D), and most of the proteins were undetectable after two days of incubation.

204 We also generated complemented cell lines expressing constitutively an additional copy of *TgNFS2*
205 and *TgISU1* from the *uracil phosphoribosyltransferase* (*UPRT*) locus from a *tubulin* promoter in their
206 respective conditional mutant backgrounds (Figure S5A, B). We confirmed by semi-quantitative RT-
207 PCR (Figure S5C) that the transcription of *TgNFS2* and *TgISU1* qenes was effectively repressed in the
208 cKD cell lines upon addition of ATc, whereas the corresponding complemented cell lines exhibited a
209 high transcription level regardless of ATc addition (due to the expression from the strong *tubulin*
210 promoter).

211 We next evaluated the consequences of TgNFS2 and TgISU1 depletion on *T. gondii* growth in vitro.
212 First, to assess the impact on the parasite lytic cycle, the capacity of the mutants and complemented
213 parasites to produce lysis plaques was analyzed on a host cells monolayer in absence or continuous
214 presence of ATc for 7 days (Figure 4A, B). Depletion of both proteins completely prevented plaque
215 formation, which was restored in the complemented cell lines. To assess whether this defect in the
216 lytic cycle is due to a replication problem, all cell lines were preincubated in absence or presence of
217 ATc for 48 hours and released mechanically, before infecting new host cells and growing them for an
218 additional 24 hours in ATc prior to parasite counting. We noted that incubation with ATc led to an
219 accumulation of vacuoles with fewer parasites, yet that was not the case in the complemented cell
220 lines (Figure 4C, D). Overall, these data show that either TgNFS2 or TgISU1 depletion impacts parasite
221 growth.

222 Then, we sought to assess if the viability of the mutant parasites was irreversibly affected. We thus
223 performed another series of plaque assays, but at the end of the 7-day incubation, we washed out
224 the ATc, incubated the parasites for an extra 7 days in the absence of ATc and evaluated plaque
225 formation (Figure 4E). In these conditions, cKD TgNFS2-HA parasites displayed very small plaques
226 suggesting their viability was irreversibly impacted. In contrast, cKD TgISU1-HA parasites showed
227 plaques, suggesting parasite growth had at least partly resumed after ATc washout, while host cell

228 lysis remained limited if the drug was kept continuously during the same period of time. This
229 suggests that although depletion of TgISU1 has a marked impact on parasite growth, it is not
230 completely lethal.

231 We performed IFAs to assess possible morphological defects that may explain the impaired growths
232 of cKD TgNFS2-HA and cKD TgISU1-HA parasites. We stained the apicoplast and mitochondrion of
233 parasites kept in the continuous presence of ATc for several days. cKD TgNFS2-HA parasites managed
234 to grow and egress after three days and were seeded onto new host cells, where there were kept for
235 two more days in the presence of ATc. During this second phase of intracellular development, and in
236 accordance with the replication assays (Figure 4C), growth was slowed down considerably. Strikingly,
237 while the mitochondrial network seemed normal, we noticed a progressive loss of the apicoplast
238 marker TgCPN60 (Figure 5A), which was quantified (Figure 5B). As this could reflect a specific impact
239 on this protein marker rather than a loss of the organelle, we also stained the parasites with
240 fluorescent streptavidin, which mainly detects the biotinylated apicoplast protein acetyl-CoA
241 carboxylase [48], confirming a similar loss of signal (Figure S6). This suggests there is a general impact
242 of TgNFS2 depletion on the organelle. The growth kinetics we observed for this mutant are
243 consistent with the "delayed death" effect observed in apicoplast-defective parasites [6,49,50]. On
244 the other hand, we were able to grow cKD TgISU1-HA parasites for five days of continuous culture:
245 they developed large vacuoles and showed little sign of egress from the host cells (Figure 5C). Both
246 the mitochondrion and the apicoplast appeared otherwise normal morphologically. These large
247 vacuoles could reflect a defect in the parasite egress stage of the lytic cycle [51]. We thus performed
248 an egress assay on cKD TgISU1-HA parasites that were kept for up to five days in the presence of ATc,
249 and they were able to egress normally upon addition of a calcium ionophore (Figure 5D). These large
250 vacuoles are also reminiscent of cyst-like structures [52], so alternatively this may reflect
251 spontaneous stage conversion. Cysts are intracellular structures that contain the slow-growing form
252 of *T. gondii*, called the bradyzoite stage (which is responsible for the chronic phase of the disease),
253 and they may appear even during in vitro growth in particular stress conditions [53]. Yet, this mutant
254 cell line was generated in a type I *T. gondii* strain, which is associated with acute toxoplasmosis in the
255 mouse model [54], and typically does not spontaneously form cysts. So, to be confirmed this
256 hypothesis needed further investigations, as we will see later in the manuscript.

257 In any case, our data show that interfering with the plastidic and mitochondrial Fe-S protein
258 pathways both had important consequences on parasite growth, but had a markedly different impact
259 at a cellular level.

260

261 **Use of label-free quantitative proteomics to identify pathways affected by TgNFS2 or TgISU1**
262 **depletion**

263 There is a wide variety of eukaryotic cellular processes that are depending on Fe-S cluster proteins.
264 To get an overview of the potential *T. gondii* Fe-S proteome, we used a computational tool able to
265 predict metal-binding sites in protein sequences [55], and performed subsequent manual curation to
266 refine the annotation. We identified 64 proteins encompassing various cellular functions or
267 metabolic pathways that included, beyond the Fe-S synthesis machinery itself, several DNA and RNA
268 polymerases, proteins involved in redox control and electron transfer, and radical S-
269 adenosylmethionine (SAM) enzymes involved in methylation and methylthiolation (Table S2).
270 HyperLOPIT data or manual curation helped us assign a putative localization for these candidates. A
271 considerable proportion (19%) of these were predicted to localize to the nucleus, where many
272 eukaryotic Fe-S proteins are known to be involved in DNA replication and repair [56]. Yet, strikingly,

273 most of the predicted Fe-S proteins likely localize to the endosymbiotic organelles. Several (19%) are
274 predicted to be apicoplast-resident proteins, including radical SAM enzymes lipoate synthase (LipA)
275 [57] and MiaB, a tRNA modification enzyme [58], as well as the IspG and IspH oxidoreductases of the
276 non-mevalonate isoprenoid pathway [59]. Finally, for the most part (43%), candidate Fe-S proteins
277 were predicted to be mitochondrial, with noticeably several important proteins of the respiratory
278 chain (SDHB, the Fe-S subunit of the succinate dehydrogenase complex, Rieske protein and
279 TgApiCox13) [60–62], but also enzymes involved in other metabolic pathways such as heme or
280 molybdopterin synthesis. CRISPR/Cas9 fitness scores [38] confirmed many of these putative Fe-S
281 proteins likely support essential functions for parasite growth.

282 We sought to confirm these results experimentally. Thus, in order to uncover the pathways primarily
283 affected by the depletion of TgISU1 and TgNFS2, and to identify potential Fe-S protein targets, we
284 conducted global label-free quantitative proteomic analyses. Like most plastidic or mitochondrial
285 proteins, candidate Fe-S acceptors residing in these organelles are nuclear-encoded and thus need to
286 be imported after translation and have to be unfolded to reach the stroma of the organelle. This not
287 only implies the addition of the Fe-S cofactor should happen locally in the organelle, but also that this
288 may have a role in proper folding of these proteins. We thus assumed that disrupting a specific
289 pathway may have a direct effect on the stability and expression levels of local Fe-S proteins. Cellular
290 downstream pathways or functions may also be affected, while other pathways may be upregulated
291 in compensation. Parasites were treated for two days with ATc (TgISU1-HA) or three days (cKD
292 TgNFS2-HA, as it takes slightly longer to be depleted, Figure 3A), prior to a global proteomic analysis
293 comparing protein expression with the ATc-treated TATi ΔKu80 control. For each mutant, we
294 selected candidates with a log2(fold change) ≤-0.55 or ≥0.55 (corresponding to a ~1.47-fold change in
295 decreased or increased expression) and a p-value <0.05 (ANOVA, *n*=4 biological replicates) (Tables S3
296 and S4, Figure 6A, B). To get a more exhaustive overview of proteins whose amounts varied
297 drastically, we completed this dataset by selecting some candidates that were consistently and
298 specifically absent from the mutant cell lines or only expressed in these (Tables S3 and S4).

299 Overall, depletion of TgISU1 led to a higher variability in protein expression and while the pattern of
300 expression was essentially specific for the respective mutants, a number of shared variant proteins
301 were found (Figure 6C, Table S5). For instance, common lower expressed candidates include a SAM
302 synthase, possibly reflecting a general perturbation of SAM biosynthesis upon loss of function of Fe-
303 S-containing radical SAM enzymes [63]. Using dedicated expression data [64,65] available on
304 ToxoDB.org we realized that, strikingly, many of the common variant proteins were stage-specific
305 proteins (Table S5). For instance, the protein whose expression went down the most is SAG-related
306 sequence (SRS) 19F. The SRS family contains GPI-anchored surface antigens related to SAG1, the first
307 characterized *T. gondii* surface antigen, and whose expression is largely stage-specific [66]. This
308 protein, SRS19F, may be most highly expressed in stages present in the definitive host [65,67].
309 Conversely, SRS44, also known as CST1 and one of the earliest marker of stage conversion to
310 bradyzoites [68], was upregulated in both mutants. Several other bradyzoite proteins whose
311 expression increased included Ank1, a tetratricopeptide-repeat protein highly upregulated in the
312 cyst-stages but not necessary for stage conversion [69], aspartyl protease ASP1, an α-galactosidase,
313 as well as several dense granule proteins (GRA). Dense granules are specialized organelles that
314 secrete GRA proteins that are known to participate in nutrient acquisition, immune evasion, and host
315 cell-cycle manipulation. Many GRA have been characterized in the tachyzoite stage, but several are
316 stage-specific and expressed in bradyzoites [70]. It should be noted that bradyzoite-specific proteins
317 were generally much strongly expressed upon TgISU1 depletion than TgNFS2 depletion.
318 Nevertheless, altogether these results show that altering either the plastidic or the mitochondrial Fe-

319 S cluster synthesis pathway led to an initial activation of the expression of some markers of the
320 bradyzoite stage, whose involvement in the stress-mediated response is well documented [53].

321

322 **Depletion of TgNFS2 has an impact on the apicoplast, but also beyond the organelle**

323 We next focused on proteins that varied specifically upon depletion of TgNFS2 (Table S3). Using the
324 hyperLOPIT data available on ToxoDB.org, we assessed the putative localization of the candidates
325 (Figure 6D, Figure S7A) and we also defined putative functional classes based on manual curation
326 (Figure 6A, Figure S7B). Surprisingly, few apicoplast proteins were impacted. This could reflect a
327 limited impact on apicoplast Fe-S apoproteins, but this is in contradiction with the late, yet
328 pronounced, effect we see on the organelle in the absence of TgNFS2 (Figure 5A, B). There might also
329 be a bias due to an overall low protein abundance: less than half of the apicoplast candidates of the
330 predicted Fe-S proteome (Table S2) were robustly detected even in the control for instance, including
331 our target protein TgNFS2. Finally, of course it is possible that depletion of Fe-S clusters, while
332 impacting the functionality of target proteins, did not have a considerable effect on their abundance.
333 We sought to verify this for apicoplast stroma-localized LipA, a well-established and evolutionarily-
334 conserved Fe-S cluster protein, which was found to be only marginally less expressed in our analysis
335 (Table S3). LipA is responsible for the lipoylation of a single apicoplast target protein, the E2 subunit
336 of the pyruvate dehydrogenase (PDH) [32]. Using an anti-lipoic acid antibody on cKD TgNFS2-HA
337 protein extracts, we could already see a marked decrease in lipoylated PDH-E2 after only one day of
338 ATc incubation (Figure 7A). This was not due to a general demise of the apicoplast as it considerably
339 earlier than the observed loss of the organelle (Figure 5A, B), and levels of the CPN60 apicoplast
340 marker were clearly not as markedly impacted (Figure 7A). This is also unlikely to reflect a general
341 decrease of TgPDH-E2 levels upon TgNFS2 knock-down, as our quantitative proteomics data, which
342 was performed after 3 days of ATc incubation, show the same amount of unique peptides for TgPDH-
343 E2 (32 ± 2.5 for the control and 32.25 ± 2.75 for the mutant, ~60% of sequence coverage). This
344 finding suggests apicoplast Fe-S-dependent activities may be specifically affected in our mutant,
345 which would happen before observing the general demise and loss of the organelle. Long term
346 incubation of cKD TgNFS2-HA parasites with ATc and co-staining with apicoplast and inner membrane
347 complex (IMC) markers, revealed general cell division defects, including organelle segregation
348 problems and an abnormal membranous structures (Figure 7B). Overall, this suggests impacting the
349 Fe-S cluster synthesis pathway in the apicoplast had important metabolic consequences beyond the
350 organelle itself.

351

352 **Depletion of TgISU1 impacts the mitochondrial respiratory chain**

353 We also analyzed the proteins whose abundance changed upon TgISU1 depletion (Table S4). Again,
354 we used hyperLOPIT data to determine the localization of variant proteins (Figure 6E, Figure S8A) and
355 we also inferred their potential function from GO terms or manual curation (Figure 6B, Figure S8B).
356 Depletion of TgISU1 had a notable impact locally, as numerous mitochondrial proteins were found in
357 lower abundance. Remarkably, most of these proteins were identified as members of the
358 mitochondrial respiratory chain: while our proteomic study detected peptides corresponding to as
359 much as 92% of the hyperLOPIT-predicted mitochondrial membrane and soluble proteins, 12% of
360 these were found to be significantly less expressed upon TgISU1 depletion, 60% of which are known
361 mitochondrial ETC components (Figure 6A, Figure 8A, Table S4). This suggests a specific effect of
362 TgISU1 depletion on the mitochondrial ETC. This ETC comprises four complexes in Apicomplexa
363 (which typically lack complex I), in which several Fe-S proteins have important function. As

364 mentioned earlier, they include the Fe-S subunit of the succinate dehydrogenase complex (SDHB,
365 part of complex II), the Rieske protein (part of complex III) and TgApiCox13 (part of complex IV) [60–
366 62]. Not only these three Fe-S cluster proteins were found to be less expressed upon TgISU1
367 depletion, but about 60% and 80% of complexes III and IV components (including recently
368 characterized parasite-specific subunits [61,62]), respectively, were also significantly less abundant
369 (Table S4, Figure 8A). The impact on components of complexes III and IV beyond their respective Fe-
370 S-dependent subunits is not surprising: as shown by others in *T. gondii* depletion of selected
371 members of a mitochondrial ETC complex can result in stalled assembly or impaired stability of the
372 whole complex [60–62,71].

373 We sought to verify the impact of TgISU1 depletion on proteins of the mitochondrial respiratory
374 chain by tagging two candidates, TgSDHB and TgApiCox13. In order to do this, due to the lack of
375 efficient selectable marker in the cKD TgISU1-HA cell line, we first had to generate a new
376 independent cKD TgISU1 untagged mutant from the TATi ΔKu80 cell line (Figure S9A, B). In this cell
377 line, we verified proper regulation of *TgISU1* expression by ATc (Figure S9C) and impact of TgISU1
378 depletion on parasite growth (Figure S9D). In this cKD TgISU1 mutant, a sequence coding for a C-
379 terminal triple HA epitope tag was inserted at the endogenous *TgSDHB* or *TgApiCox13* locus by
380 homologous recombination (Figure S10). We then incubated these parasites with ATc for three days
381 and used an anti-HA antibody to detect and quantify the proteins of interest by IFA (Figure 8B) and
382 immunoblot (Figure 8C). In accordance with the quantitative proteomics data, both TgSDHB and
383 TgApiCox13 were found to be less expressed in absence of TgISU1.

384 This suggested the mitochondrial membrane potential and consequently the respiratory capacity of
385 the mitochondrion were likely altered in the absence of a functional mitochondrial Fe-S cluster
386 synthesis pathway. To verify this, we performed flow cytometry quantification using JC-1, a
387 monomeric green fluorescent carbocyanine dye that accumulates as a red fluorescent aggregates in
388 mitochondria depending on their membrane potential (Figure 8D). Depletion of TgISU1 led to a
389 marked decrease of the parasite population displaying a strong red signal (Figure 8D). The effect was
390 maximal after two days of ATc treatment and not further increased by a four-day treatment, which is
391 consistent with the quantitative proteomics data already showing strong impact on proteins from
392 complexes II, III and IV after only two days of ATc treatment. It should be noted that although we
393 believe the drop in mitochondrial membrane potential is likely due to a specific alteration of the
394 respiratory chain, it may also be due to a loss of parasite viability. Reassuringly, our results are in line
395 with the recent findings obtained by Aw et al., who generated a mutant of mitochondrial Fe-S cluster
396 synthesis (by depleting TgNFS1), and observed a sharp decrease in TgSDHB abundance and a clear
397 drop in mitochondrial O_2 consumption rate [25].

398 Concomitantly to the lesser expression of mitochondrial respiratory chain subunits, the proteomics
399 analysis revealed TgISU1 depletion induced a significant increase in cytosolic enzymes involved in
400 glycolysis, as well as its branching off pentose phosphate pathway (Figure 8A, B, Table S4). The
401 upregulation of glycolytic enzymes potentially reflects a metabolic compensation for mitochondrial
402 defects in energy production due to the impairment of the respiratory chain. Other proteins whose
403 abundance was markedly decreased were predicted to be cytoplasmic or nuclear, including proteins
404 involved in DNA repair and replication (Table S4), which is perhaps unsurprising as the cytosolic CIA
405 Fe-S cluster assembly pathway is supposedly dependent from the ISC pathway [24]. Finally, the
406 changes in abundance of several RNA-binding proteins involved in mRNA half-life or
407 transcription/translation regulation may also reflect adaptation to a stress (Table S4).

408

409 **Depletion of TgISU1 initiates conversion into bradyzoites**

410 Another feature highlighted by the quantitative proteomics analysis of the TgISU1 mutant is indeed
411 the change in the expression of stage-specific proteins (Table S4). The expression of several
412 bradyzoite-specific proteins including GRAs and proteins of the SRS family, was strongly increased. At
413 the same time, some tachyzoite-specific SRS and GRA proteins were found to be less expressed. This
414 was supporting the idea that intracellularly developing parasites lacking TgISU1 may convert into
415 bona fide cyst-contained bradyzoites, as suggested by our initial morphological observations (Figure
416 5C). To verify this experimentally, we used a lectin from the plant *Dolichos biflorus* (DBL), which
417 recognizes the SRS44/CST1 glycoprotein that is exported to the nascent wall of differentiating cysts
418 [68]. We could see that during continuous growth of cKD TgISU1-HA parasites in the presence of ATc,
419 there was an increasing number of DBL-positive structures (Figure 9A). This was quantified during the
420 first 48 hours of intracellular development (Figure 9B) and, interestingly, was shown to mimic the
421 differentiation induced by nitric oxide, a known factor of stage conversion [72], and a potent
422 damaging agent of Fe-S clusters [73]. We combined RNAseq expression data for tachyzoite and
423 bradyzoite stages [65] to establish a hierarchical clustering of the SRS proteins detected in our
424 quantitative proteomics experiments for the two mutants (Figure 9C). This clearly confirmed a strong
425 increase in the expression of bradyzoite-specific SRS in the TgISU1 mutant. As mentioned earlier,
426 some were also upregulated in the TgNFS2 mutant but in much lesser proportions. The strongest
427 increase in bradyzoite-specific SRS expression upon TgNFS2 depletion was for SRS44/CST1, which
428 happens to be the protein DBL preferentially binds to [68]. However, contrarily to the TgISU1 mutant,
429 labelling experiments did not indicate any detectable increase in DBL recruitment in the TgNFS2
430 mutant (Figure 9B), confirming that impairing the plastidic Fe-S center synthesis pathway does not
431 trigger full stage conversion.

432 Stage conversion is a progressive process that happens over the course of several days, as it involves
433 the expression of distinct transcriptomes and proteomes [53]. Markers for specific steps of in vitro
434 cyst formation had been previously described [74], so we have used several of these to check the
435 kinetics of stage conversion in the TgISU1-depleted parasites. We kept the cKD TgISU1-HA parasites
436 for up to 14 days in the presence of ATc and tested for the presence of SAG1 (tachyzoite maker), DBL
437 (early bradyzoite marker), P18/SAG4 (intermediate bradyzoite marker) and P21 (late bradyzoite
438 marker) (Figure 9D). After 7 days of ATc treatment, the DBL-positive cyst contained parasites that
439 were still expressing SAG1 and not yet SAG4, whereas after 14 days parasites with SAG4 labelling
440 were found, but there was still a residual SAG1 expression; expression of late marker P21 was,
441 however, never detected. This suggests stage conversion of these parasites progresses beyond the
442 appearance of early cyst wall markers, but not only it does so with slow kinetics, but it seems
443 incomplete. In fact, observation of DBL-positive cysts showed a marked decrease in their mean size
444 between the 7 and 14 days timepoints (Figure 9D). This suggests incomplete conversion may be
445 leading to subsequent reactivation/reinvasion events. The smaller cyst size may also suggest a lack of
446 fitness in the long term for TgISU1-depleted parasites.

447

448 **Lack of lethality and initiation of stage conversion are features shared by other mitochondrial**
449 **mutants**

450 As impairment of the mitochondrial ETC and stage conversion are the two main features observed
451 for the TgISU1 mutant, it raised the possibility the former may be involved in triggering the latter. We
452 thus sought to evaluate in more details viability and differentiation of other mitochondrial mutants.
453 We used the ATc-regulatable cKD cell line for TgQCR11 [62], a complex III subunit found less

454 abundant in absence of TgISU1 (Figure 8A), and which was found by others to be essential for
455 mitochondrial respiration and parasite growth [61,62]. We also included in our study an ATc-
456 regulatable cKD cell line for TgmS35, a mitoribosomal protein whose depletion impacts organelle
457 morphology and function (including mitochondrial respiration), and overall parasite fitness [75].

458 Like for TgISU1 (Figure 4E), we assessed whether or not the fitness phenotype of these mutants was
459 reversible by performing plaque assays in the presence of ATc for 7 days, and then monitored plaque
460 formation for another 7 days upon drug removal (Figure 10A). The TgQCR11 mutant behaved very
461 similarly to the TgISU1 mutant, with virtually no plaques formed when incubated with ATc, while it
462 was able to reactivate the lytic cycle upon ATc washout. The TgmS35 mutant seemed less affected by
463 protein depletion: not only it generated small plaques after 7 days in the presence of ATc, but
464 whether or not the drug was washed out, prolonged incubation led to large lysis plaques in the host
465 cells. Overall, this experiment showed that mitochondrial mutants, whether they are affected in a
466 metabolic or more structural function, remain essentially viable. The similarity between the TgISU1
467 and the TgQCR11 mutant suggested the latter may be switching to a slow-growing but still viable
468 bradyzoite stage. The slowed-down, but less hampered progression through the lytic cycle of the
469 TgmS35 mutant suggested it might retain more tachyzoite-like growth kinetics.

470 To investigate the ability of these mutants to form cysts, we performed IFAs with specific bradyzoite
471 markers, like we did previously for the cKd TgISU1-HA cell line (Figure 9A, B). We first looked for the
472 recruitment of DBL to parasite-containing vacuoles during the first 48 hours of protein depletion,
473 (Figure 10B, C). As a control, we also treated TATi ΔKu80 parasites with atovaquone, an inhibitor of
474 the mitochondrial ETC that was previously shown to trigger stage conversion [76]. Interestingly, like
475 the atovaquone-treated TATi ΔKu80 parasites and the TgISU1 mutant (Figure 9A and B), treatment of
476 both TgQCR11 and TgmS35 mutants with ATc seemed to trigger stage conversion, as illustrated by an
477 increase in DBL staining of vacuoles over time (Figure 10B and C). When then tried to evaluate
478 conversion over a longer period by keeping the parasites for up to 14 days in the presence of ATc
479 (Figure 10D). For the TgmS35 mutant, this was achieved by using very low doses of parasite
480 inoculum, which allowed preserving some host cells in spite of the extensive lysis caused by the
481 parasites. Like for the TgISU1 mutant, even long term parasite did not allow complete disappearance
482 of the SAG1 tachyzoite marker in the TgQCR11 and TgmS35 mutants, and staining of the late
483 bradyzoites marker P21 was not observed. However, while a few DBL-labelled cysts remained in the
484 TgmS35 culture after 14 days of ATc treatment, they very rarely showed staining with the
485 intermediate bradyzoite marker P18/SAG4. On the contrary, substantial staining was observed upon
486 long term depletion of TgQCR11, like we observed for the TgISU1 mutant.

487 In conclusion, our findings suggest that interfering with general function like mitochondrial
488 translation, or targeting more specifically the mitochondrial ETC, does not irreversibly impair parasite
489 viability and instead leads to an initiation of stage conversion into bradyzoites, although it may not
490 necessarily be complete.

491

492 **Discussion**

493 Because of their origin and metabolic importance, the two apicomplexan endosymbiotic organelles
494 have gathered considerable interest as potential drug targets [77,78]. It may be obvious, as for
495 example the plastid hosts several metabolic pathways which are not present in the mammalian hosts
496 of these parasites. Yet, even for conserved housekeeping functions or, in the case of the
497 mitochondrion early phylogenetic divergence, there may still be enough molecular differences to
498 allow selective chemical inhibition. In fact, several drugs used for prophylactic or curative treatments

499 against Apicomplexa-caused diseases are already targeting these organelles [79]. They are essentially
500 impacting the organellar protein synthesis by acting on the translation machinery [80], although the
501 mitochondrial ETC inhibitor atovaquone is also used to treat malaria and toxoplasmosis [81]. One
502 main difference when targeting *Plasmodium* and *Toxoplasma* by drugs is that the latter easily
503 converts into the encysted bradyzoite resistance form. It has been known for some time that
504 treatment of tachyzoites with mitochondrial inhibitors triggers stage conversion [72,76,82]. This may
505 be efficient to counteract the acute phase of toxoplasmosis, but at the same time may favour
506 persistence of the parasites in the host.

507 Here we characterized Fe-S synthesis pathways which are very similar biochemically, but are located
508 into two distinct endosymbiotic organelles, and whose inactivation has drastically different
509 consequences for parasite fitness. Fe-S clusters are ancient, ubiquitous and fundamental to many
510 cellular functions, but their synthesis by distinct biosynthetic pathways was inherited by plastids or
511 by the mitochondrion through distinct bacterial ancestors, and have thus specialized into adding
512 these cofactors to different client proteins [22]. A key function of Fe-S clusters, owing to their mid-
513 range redox potential, is electron transfer and redox reactions, mainly as components the respiratory
514 and photosynthetic ETCs. They also have important functions in stabilizing proteins, redox sensing, or
515 catalysis through SAM enzymes. Several of these are not retained in Apicomplexa, whose plastid has
516 lost its photosynthetic ability for example. Nevertheless, our prediction of the *T. gondii* Fe-S proteins
517 repertoire suggests many key functions associated with the apicoplast or the mitochondrion are
518 likely to be affected by a perturbation of Fe-S assembly (Table S2).

519 For the apicoplast, these include lipoic acid or isoprenoid synthesis. Inactivation of the apicoplast-
520 located TgNFS2 had a late but marked effect on the organelle itself, as it led ultimately to a partial
521 loss of the apicoplast, which is consistent with the phenotype observed when disrupting the SUF
522 pathway in *Plasmodium* [26]. IspG and IspH, which are key Fe-S-dependent enzymes of the non-
523 mevalonate isoprenoid synthesis pathway [59], were only found marginally less expressed in our
524 quantitative analysis after TgNFS2 depletion. However, our proteomics dataset provided indirect
525 clues that their function may be impacted. Isoprenoid synthesis is vital for *T. gondii* tachyzoites [33],
526 and it has implication beyond the apicoplast, as prenylated proteins or isoprenoid precursors are
527 involved in more general cellular processes including intracellular trafficking or mitochondrial
528 respiration [83]. Isoprenoids are for instance important for synthesizing ubiquinone/coenzyme Q,
529 and the single predicted mitochondrial candidate that was significantly less expressed upon TgNFS2
530 depletion is a putative UbiE/COQ5 methyltransferase, involved in synthesis of this co-factor [84].
531 Isoprenoids are also important for dolichol-derived protein glycosylation and
532 glycosylphosphatidylinositol (GPI)-anchor biosynthesis, and interestingly the three putative rhoptry-
533 localized candidates significantly less expressed in the TgNFS2 mutant (Table S3) are predicted to be
534 GPI-anchored and/or glycosylated. Overall, this might be an indication that TgNFS2 depletion impacts
535 isoprenoid synthesis in the apicoplast, which in turn would impact other metabolic pathways.

536 Impairing isoprenoid synthesis does not, however, necessarily lead to a loss of the organelle [26].
537 There may thus be another explanation for this phenotype. Interestingly, we could show that
538 perturbing the SUF pathway, which is supposedly important for Fe-S-containing enzyme LipA,
539 impacts the lipoylation of the E2 subunit of the apicoplast-located PDH (Figure 7A). The PDH complex
540 catalyzes the production of acetyl-CoA, which is the first step of the FASII system, and perturbation of
541 either the PDH or other steps of the FASII system leads to a loss of the organelle and severely impairs
542 fitness of the parasites [33,85]. Interestingly, long term depletion of TgISU1 leads to cell division
543 problems, and affects membrane compartments such as the IMC (Figure 7B), which are defects
544 previously observed in parasites where the FASII system has been genetically- or chemically-

545 disrupted [86–88]. Our quantitative proteomic analysis shows potential compensatory mechanisms
546 may be used by the parasites in response this early perturbation of the apicoplast lipid metabolism
547 that precedes organelle loss. Tachyzoites are indeed known to be able to use exogenous lipid sources
548 to adapt metabolically [85,87] and, interestingly, upon depletion of TgNFS2 we observed a pattern of
549 overexpression for ER-located enzymes involved in the synthesis of several phospholipids and
550 ceramides (Figure 6A and D, Table S3). These lipids are usually synthesized in the ER from apicoplast-
551 generated precursors, as both organelles cooperate for FA and phospholipid (PL) synthesis [89]. Yet,
552 the ER-localized PL-synthesis machinery can also use FA scavenged from the host [90]. The increased
553 expression of ER-localized lipid-related enzymes may thus reflect an increased synthesis, potentially
554 from exogenous lipid precursors, in compensation for a defect in the apicoplast-localized machinery.
555 In spite of this potential compensation mechanism, it seems the alteration of the SUF pathway in *T.*
556 *gondii* has such a profound impact that it ultimately leads to the irreversible demise of the parasites
557 (Figure 4E). It would be interesting to use recently described approaches like stable isotope labelling
558 of lipid precursors combined to lipidomic analysis [87], to investigate in the SUF pathway mutant the
559 potential changes in de novo synthesis of FA or in lipid scavenging from the host.

560 In the mitochondrion, important pathways potentially involving Fe-S proteins include the respiratory
561 ETC, the TCA cycle, as well as molybdenum and heme synthesis (Table S2). Accordingly, perhaps the
562 most obvious consequence of disrupting the ISC pathway was the profound impact on the
563 mitochondrial respiratory capacity, as evidenced experimentally by measuring the mitochondrial
564 membrane potential (Figure 8D), and supported by quantitative analyses showing a clear drop in
565 expression of many respiratory complex proteins (Figure 8A, B, and C, Table S4). This is also in line
566 with the recent description of another mitochondrial Fe-S cluster synthesis mutant that showed a
567 marked alteration of its respiratory capacity [25]. Although the mitochondrion, through the TCA cycle
568 and the respiratory chain/oxidative phosphorylation, contributes to energy production in tachyzoites
569 [91], the glycolytic flux is also believed to be a major source of carbon and energy for these parasites
570 [92]. Thus, rather coherently, as highlighted by our quantitative proteomic analysis, disruption of the
571 ISC pathway led to a potential overexpression of glycolytic enzymes concurrently with the lower
572 expression of mitochondrial ETC components (Figure 6B, Table S4). The possible overexpression of
573 enzymes of the pentose phosphate pathway, which is branching off from glycolysis and is providing
574 redox equivalents and precursors for nucleotide and amino acid biosynthesis, is also potentially
575 indicative of a higher use of glucose in these conditions. The metabolic changes encountered by ISC-
576 deficient parasites do not cause their rapid demise, as they are able to initiate conversion to the
577 bradyzoite stage, which has been suggested to rely essentially on glycolysis for energy production
578 [93]. Our analysis of the viability of other mitochondrial mutants confirmed results obtained by
579 others showing that the organelle, and in particular the ETC, seem important for parasite fitness
580 [61,62,75]. Yet, perhaps because of their metabolic flexibility, we have shown that mutant parasites
581 seem to retain the ability to survive as tachyzoites, or initiate a switch to bradyzoites.

582 The inactivation of the ISC pathway likely has consequences on other important cellular
583 housekeeping functions besides mitochondrial metabolism. In other eukaryotes, the ISC pathway
584 provides a yet unknown precursor molecule as a sulfur provider for the cytosolic CIA Fe-S cluster
585 assembly pathway [24]. The ISC pathway thus not only governs the proper assembly of mitochondrial
586 Fe-S proteins, but also of cytoplasmic and nuclear ones. Our quantitative proteomics data suggests it
587 is also the case in *T. gondii*, as several putative nuclear Fe-S proteins involved in gene transcription
588 (such as DNA-dependent RNA polymerases) or DNA repair (like DNA endonulease III) were found to
589 be impacted by TgISU1 depletion. The CIA pathway has recently been shown to be important for
590 tachyzoite proliferation [25], and several of the cytoplasmic or nuclear Fe-S cluster-containing
591 proteins are likely essential for parasite viability. It is thus possible that, in spite of their conversion to

592 a stress-resistant form, the long-term viability of TgISU1 parasites could be affected beyond recovery.
593 In vivo experiment in the mouse model may be used to assess this.

594 The transition from tachyzoite to bradyzoite is known to involve a considerable change in gene
595 expression [64,65], and it takes several days of in vitro differentiation-inducing conditions to obtain
596 mature cysts [94,95]. Quantitative proteomic analysis showed that TgISU1-depleted parasites rapidly
597 display a high expression of bradyzoite-specific surface antigens and GRA markers (Table S4, Figure
598 9C). In all the mitochondrial mutants investigated in this study, long term perturbation of the
599 organelle led to the appearance of parasite-containing structures with typical cyst-like morphology
600 (Figure 5, Figure 9, Figure 10). However, using specific antibodies against early or late bradyzoite
601 markers, the differentiating parasites never appeared to reach a fully mature bradyzoite stage
602 (Figures 9 and 10). Also, contrarily to the ETC mutants (TgQCR11 and TgISU1), the mitochondrial
603 translation mutant (TgmS35), while seemingly initiating conversion to bradyzoite, largely continued
604 to thrive with almost tachyzoite growth dynamics (Figure 10A). However, as the mitochondrion
605 encodes three proteins that are subunits of mitochondrial ETC complexes III (cytochrome b) and IV
606 (CoxI and III), this mutant should also be supposedly impacted for ETC function. This apparent
607 discrepancy might then be explained by a looser control of down-regulation of protein expression, or
608 by compensatory mechanisms that may be specifically at play in this particular mutant. It is also
609 possible that more directly targeting the ETC is a much stronger inducer of differentiation, and thus
610 different mitochondrial mutants may behave differently regarding stage conversion. Importantly,
611 one main reason potentially explaining the incomplete differentiation of these mitochondrial
612 mutants is that they were generated in a type I *T. gondii* strain that typically does not form cysts:
613 type I tachyzoites may upregulate specific bradyzoite genes and, according to some reports, produce
614 bradyzoite-specific proteins or cyst wall components, but they are largely incapable of forming
615 mature bradyzoite cysts [96]. This calls for further investigations, and in particular generating similar
616 mitochondrion-related mutants in more cystogenic type II parasites, which could be very insightful.

617 Our quantitative proteomics analysis shows that SUF-impaired parasites also seem to initiate an
618 upregulation of some bradyzoite markers early after TgNFS2 depletion. Yet, these parasites did not
619 display the hallmarks of bradyzoite morphology. They did not progress towards stage conversion and
620 instead they displayed considerable perturbation of the cell division process (Figure 7B), and
621 eventually died. Both the apicoplast and the mitochondrion have established a close metabolic
622 symbiosis with their host cell, so there are likely multiple mechanisms allowing these organelles to
623 communicate their status to the rest of the cell. This raises the question as to why mitochondrion,
624 but not apicoplast, dysfunction can lead to differentiation into bradyzoites. This may be due to
625 differences in the kinetics or the severity of apicoplast-related phenotypes that may not allow stage
626 conversion (which is typically a long process) to happen. Alternatively, there might be differentiation
627 signals specifically associated to the mitochondrion. In fact this organelle is increasingly seen as a
628 signalling platform, able to communicate its fitness through the release of specific metabolites,
629 reactive oxygen species, or by modulating ATP levels [97]. Interestingly, it was shown in other
630 eukaryotes that mitochondrial dysfunctions, such as altered oxidative phosphorylation, significantly
631 impair cellular proliferation, oxygen sensing or specific histone acetylation, yet without diminishing
632 cell viability and instead may lead to quiescent states [98–100]. Consequences of mitochondrial
633 dysfunction include a restricted energy supply and thus constitutes a metabolic challenge that can
634 trigger important cellular adaptations that ultimately determine eukaryotic cell fate and survival. Our
635 results suggest that this is also possibly the case for *T. gondii*. It is for instance quite interesting to see
636 that altering the respiratory activity of the organelle, whether it is by generating specific mutants or
637 by the use of drugs such as atovaquone, seems to lead to a similar differentiation phenotype.

638 More generally, the environmental or metabolic cues that drive specific gene expression to induce a
639 functional shift leading to conversion into bradyzoites are not fully identified. Moreover, how these
640 stimuli are integrated is also largely unknown. A high-throughput approach has allowed the recent
641 identification of a master transcriptional regulator of stage conversion [101], but how upstream
642 events are converted into cellular signals to mobilize the master regulator is still an important, yet
643 unresolved, question. Translational control [102] may play a role in regulating this factor in the
644 context of the integrated stress response [103]. In fact, an essential part of the eukaryotic cell stress
645 response occurs post-transcriptionally and is achieved by RNA-binding proteins [104]. Interestingly,
646 among the proteins significantly less abundant in the spontaneously-differentiating TgISU1 mutant
647 were many RNA-binding proteins. They include components of stress granules (PolyA-binding
648 protein, PUF1, Alba1 and 2, some of which are linked to stage conversion [105–107]), which are
649 potentially involved in mRNA sequestration from the translational machinery, but also two regulators
650 of the large 60S ribosomal subunit assembly, as well as the gamma subunit of the eukaryotic
651 translation initiation factor (eIF) complex 4 (known to be down-regulated in the bradyzoite stage
652 [108]). Variation in these candidates may have a considerable impact on the translational profile and
653 on the proteostasis of differentiating parasites, and how they may help regulating stage conversion
654 in this context should be investigated further. Understanding the mechanisms that either lead to
655 encystment or death of the parasites is crucial to the development of treatments against
656 toxoplasmosis. This question is key to the pathology, because long term persistence of bradyzoites
657 and their resistance to current treatments makes them a durable threat for their human hosts.
658 Comparative studies of stress-induced or spontaneously differentiating conditional mutants may
659 bring further insights on how the parasites integrate upstream stresses or dysfunctions into global
660 regulation of stage conversion.

661

662 **Materials and methods**

663 **Parasites and cells culture.** Tachyzoites of the TATi ΔKu80 *T. gondii* strain [43], as well as derived
664 transgenic parasites generated in this study, were maintained by serial passage in human foreskin
665 fibroblast (HFF, American Type Culture Collection, CRL 1634) cell monolayer grown in Dulbecco's
666 modified Eagle medium (DMEM, Gibco), supplemented with 5% decomplemented fetal bovine
667 serum, 2-mM L-glutamine and a cocktail of penicillin-streptomycin at 100 µg/ml. The TgQCR11 [62]
668 and TgmS35 [75] conditional mutants cell lines were generously provided by the Sheiner laboratory.

669 **Bioinformatic analyses.** Sequence alignments were performed using the MUltiple Sequence
670 Comparison by Log-Expectation (MUSCLE) algorithm of the Geneious 6.1.8 software suite
671 (http://www.geneious.com). Transit peptide and localization predictions were done using IPSORT
672 (http://ipsort.hgc.jp/), Localizer 1.0.4 (http://localizer.csiro.au/), and Deeploc 1.0
673 (http://www.cbs.dtu.dk/services/DeepLoc-1.0/) algorithms.

674 The putative Fe-S proteome was predicted using the MetalPredator webserver
675 (http://metalweb.cerm.unifi.it/tools/metalpredator/) [55]. The whole complement of *T. gondii*
676 annotated proteins was downloaded in FASTA format from the ToxoDB database (https://toxodb.org
677 [36], release 45) and used for analysis in the MetalPredator webserver. Additional manual curation
678 included homology searches for known Fe-S proteins from plants (see appendix A in [109]), and
679 search for homologues in the Uniprot database (https://www.uniprot.org) that were annotated as
680 containing a Fe-S cofactor. For proteomics candidates, annotations were inferred from ToxoDB,
681 KEGG (https://www.genome.jp/kegg/)
682 and the Liverpool Library of Apicomplexan Metabolic Pathways (http://www.llamp.net/ [110]).

683 N-glycosylation predictions were done with the GlycoEP webserver
684 (http://crdd.osdd.net/raghava/glycoep/index.html). GPI anchor predictions were done with the
685 PredGPI (http://gpcr.biocomp.unibo.it/predgpi/) and GPI-SOM (http://gpi.unibe.ch/) webservers.

686 Candidate variant proteins identified by quantitative proteomics were mapped on the graphic
687 representation of the high-resolution spatial proteome map of *T. gondii* using the hyperLOPIT dataset
688 [37] (https://proteome.shinyapps.io/toxolopittzex/).

689 **Heterologous expression in *E. coli*.** Constructs for designing recombinant proteins were defined by
690 aligning TgNFS2 and TgISU1 amino acid sequences with their *E. coli* counterparts. For *TgNFS2*, a 1,438
691 bp fragment corresponding to amino acids 271-699, was amplified by polymerase chain reaction
692 (PCR) from *T. gondii* cDNA using primers ML4201/ML4012 (sequences of the primers used in this
693 study are found in Table S6). For *TgISU1*, a 393 bp fragment corresponding to amino acids 64-194,
694 was amplified by PCR from *T. gondii* cDNA using primers ML4204/ML4205. The fragments were
695 cloned into the pUC19 (Thermo Fisher Scientific) using the HindIII/BamHI and SphI/BamHI restriction
696 sites, respectively. *E. coli* mutants from the Keio collection (obtained from the The *Coli* Genetic Stock
697 Center at the University of Yale: stain numbers JW1670-1 for *SufS*, JW2513-1 for *IscU*), were
698 transformed with plasmids for expressing recombinant TgNFS2 and TgISU1 and selected with
699 ampicillin. For growth assays [40], overnight stationary phase cultures were adjusted to the same
700 starting OD_{600} of 0.6 in salt-supplemented M9 minimal media containing 0.4% glucose and varying
701 amounts of the 2,2′-Bipyridyl iron chelator (Sigma-Aldrich). Parental *E. coli* (strain K12) were
702 included as a control. Growth was monitored through OD_{600} measurement after 7, 14 and 24 hours at
703 37°C in a shaking incubator.

704 **Generation of HA-tagged TgNFS2, TgSUFE2 and TgISU1 cell lines.** The ligation independent strategy
705 [42] was used for C-terminal hemagglutinin $(HA)_3$-tagging of TgISU1. A fragment corresponding to the
706 3' end of *TgISU1* was amplified by PCR from genomic DNA, with the Q5 DNA polymerase (New
707 England BioLabs) using primers ML4208/ML4209 and inserted in frame with the sequence coding for
708 a triple HA tag, present in the pLIC-HA_3-chloramphenicol acetyltransferase (CAT) plasmid. The
709 resulting vector was linearized and 40 µg of DNA was transfected into the TATi ΔKu80 cell line to
710 allow integration by single homologous recombination, and transgenic parasites of the TgISU1-HA
711 cell line were selected with chloramphenicol and cloned by serial limiting dilution.

712 For TgNFS2 and TgSUFE2, a CRISPR-based strategy was used. Using the pLIC-HA_3-CAT plasmid as a
713 template, a PCR was performed with the KOD DNA polymerase (Novagen) to amplify the tag and the
714 resistance gene expression cassette with primers ML3978/ML3979 (*TgNFS2*) and ML4023/ML4162
715 (*TgSUFE2*), that also carry 30 bp homology with the 3′ end of the corresponding genes. A specific
716 single-guide RNA (sgRNA) was generated to introduce a double-stranded break at the 3′ of the
717 respective loci. Primers used to generate the guides were ML3948/ML3949 (*TgNFS2*) and
718 ML4160/ML4161 (*TgSUFE2*) and the protospacer sequences were introduced in the Cas9-expressing
719 pU6-Universal plasmid (Addgene, ref #52694) [38]. Again, the TATi ΔKu80 cell line was transfected
720 and transgenic parasites of the TgNFS2-HA or TgSUFE2-HA cell lines were selected with
721 chloramphenicol and cloned by serial limiting dilution.

722 **Generation of TgNFS2 and TgISU1 conditional knock-down and complemented cell lines.** The
723 conditional knock-down cell for *TgNFS2* and *TgISU1* were generated based on the Tet-Off system
724 using the DHFR-TetO7Sag4 plasmid [111].

725 For *TgISU1*, a 930 bp 5' region of the gene, starting with the initiation codon, was amplified from
726 genomic DNA by PCR using Q5 polymerase (New England Biolabs) with primers ML4212/ML4213 and

727 cloned into the DHFR-TetO7Sag4 plasmid, downstream of the anhydrotetracycline (ATc)-inducible
728 TetO7Sag4 promoter, yielding the DHFR-TetO7Sag4-TgISU1 plasmid. The plasmid was then linearized
729 and transfected into the TgISU1-HA cell line. Transfected parasites were selected with
730 pyrimethamine and cloned by serial limiting dilution. A similar approach was used to generate an
731 independent cKD TgISU1 cell line, but starting from the TATi ΔKu80 cell line instead of the TgISU1-HA
732 cell line, to allow subsequent tagging of mitochondrial candidates.

733 For *TgNFS2*, a CRISPR-based strategy was used. Using the DHFR-TetO7Sag4 plasmid as a template, a
734 PCR was performed with the KOD DNA polymerase (Novagen) to amplify the promoter and the
735 resistance gene expression cassette with primers ML4154/ML4155 that also carry 30 bp homology
736 with the 5 end of the *TgNFS2* gene. A specific sgRNA was generated to introduce a double-stranded
737 break at the 5 of the *TgNFS2* locus. Primers used to generate the guide were ML4156/ML4157 and
738 the protospacer sequences were introduced in the pU6-Universal plasmid (Addgene ref#52694) [38].
739 The *TgNFS2*-HA cell line was transfected with the donor sequence and the Cas9/guide RNA-
740 expressing plasmid and transgenic parasites were selected with pyrimethamine and cloned by serial
741 limiting dilution.

742 The cKD TgNFS2-HA and cKD TgISU1-HA cell lines were complemented by the addition of an extra
743 copy of the respective genes put under the dependence of a *tubulin* promoter at the *uracil*
744 *phosphoribosyltransferase* (*UPRT*) locus. *TgNFS2* (2097 bp) and *TgISU1* (657 bp) whole cDNA
745 sequences were amplified by reverse transcription (RT)-PCR with primers ML4576/ML4577 and
746 ML4455/ML4456, respectively. They were then cloned downstream of the *tubulin* promoter
747 sequence of the pUPRT-TUB-Ty vector [43] to yield the pUPRT-TgNFS2 and pUPRT-TgISU1plasmids,
748 respectively. These plasmids were then linearized prior to transfection of the respective mutant cell
749 lines. The recombination efficiency was increased by co-transfecting with the Cas9-expressing pU6-
750 UPRT plasmids generated by integrating *UPRT*-specific protospacer sequences (with primers
751 ML2087/ML2088 for the 3', and primers ML3445/ML3446 for the 5') which were designed to allow a
752 double-strand break at the *UPRT* locus. Transgenic parasites were selected using
753 5-fluorodeoxyuridine and cloned by serial limiting dilution to yield the cKD TgNFS2-HA comp cKD
754 TgISU1-HA comp cell lines, respectively.

755 **Generation of HA-tagged TgSDHB and TgApiCox13 cell lines.** A CRISPR-based strategy was used.
756 Using the pLIC-HA_3-CAT plasmid as a template, a PCR was performed with the KOD DNA polymerase
757 (Novagen) to amplify the tag and the resistance gene expression cassette with primers
758 ML5116/ML5117 (*TgSDHB*) and ML5114/ML5115 (*TgApiCox13*), that also carry 30 bp homology with
759 the 3 end of the corresponding genes. A specific sgRNA was generated to introduce a double-
760 stranded break at the 3 of the respective loci. Primers used to generate the guides were
761 ML4986/ML4987 (*TgSDHB*) and ML4984/ML4985 (*TgApiCox13*) and the protospacer sequences were
762 introduced in the Cas9-expressing pU6-Universal plasmid (Addgene, ref #52694) [38]. The cKD TgISU1
763 cell line was transfected and parasites were selected with chloramphenicol and cloned by serial
764 limiting dilution.

765 **Immunoblot analysis.** Protein extracts from 10^7 freshly egressed tachyzoites were prepared in
766 Laemmli sample buffer, separated by SDS-PAGE and transferred onto nitrocellulose membrane using
767 the BioRad Mini-Transblot system according to the manufacturer's instructions. Rat monoclonal
768 antibody (clone 3F10, Roche) was used to detect HA-tagged proteins. Other primary antibodies used
769 were rabbit anti-lipoic acid antibody (ab58724, Abcam), mouse anti-SAG1 [112], rabbit anti-CPN60
770 [113] and mouse anti-actin [114]. Protein quantification was performed by band densitometry using
771 FIJI (https://imagej.net/software/fiji/).

772 **Immunofluorescence microscopy.** For immunofluorescence assays (IFA), intracellular tachyzoites
773 grown on coverslips containing HFF monolayers, were either fixed for 20 min with 4% (w/v)
774 paraformaldehyde (PFA) in PBS and permeabilized for 10 min with 0.3% Triton X-100 in PBS or fixed
775 for 5 min in cold methanol (for the use of cyst-specific antibodies). Slides/coverslips were
776 subsequently blocked with 0.1% (w/v) BSA in PBS. Primary antibodies used (at 1/1,000, unless
777 specified) to detect subcellular structures were rabbit anti-CPN60 [113], mouse monoclonal anti-F1-
778 ATPase beta subunit (gift of P. Bradley), mouse monoclonal anti-GRA3 [115], rabbit anti-TgHSP28
779 [116], rabbit anti-GAP45 [117], mouse monoclonal anti-SAG1 [112], anti SAG4/P18 (diluted 1/200, T8
780 3B1) and anti P21 (diluted 1/200, T8 4G10) [118]. Rat monoclonal anti-HA antibody (clone 3F10,
781 Roche) was used to detect epitope-tagged proteins. Staining of DNA was performed on fixed cells by
782 incubating them for 5 min in a 1 µg/ml 4,6-diamidino-2-phenylindole (DAPI) solution. All images were
783 acquired at the Montpellier RIO imaging facility from a Zeiss AXIO Imager Z1 epifluorescence
784 microscope driven by the ZEN software v2.3 (Zeiss). Z-stack acquisition and maximal intensity
785 projection was performed to visualize larger structures such as in vitro cysts. Adjustments for
786 brightness and contrast were applied uniformly on the entire image.

787 **Plaque assay.** Confluent monolayers of HFFs were infected with freshly egressed parasites, which
788 were left to grow for 7 days in the absence or presence of ATc (added to a final concentration of 1
789 µg/ml). They were then fixed with 4% v/v PFA and plaques were revealed by staining with a 0.1%
790 crystal violet solution (V5265, Sigma-Aldrich). For the washout experiments, after 7 days the culture
791 medium was removed from the wells and one gentle wash was performed with Hanks' Balanced Salt
792 Solution (HBSS), taking care not to disturb the cells; then new DMEM medium containing or not ATc
793 was added for another 7-day incubation, before termination of the experiment by PFA fixation and
794 crystal violet staining.

795 **Egress assay.** *T. gondii* tachyzoites were grown for 40 (without ATc) or 120 (with ATc) hours on HFF
796 cells with coverslips in 24-well plates. The infected host cells were incubated for 7 min at 37°C with
797 DMEM containing 3 µM of calcium ionophore A23187 (C7522, Sigma-Aldrich) prior to fixation with
798 4% PFA. Immunofluorescence assays were performed as previously described [119]: the parasites
799 and the parasitophorous vacuole membrane were labelled with anti-GAP45 and anti-GRA3,
800 respectively. The proportion of egressed and non-egressed vacuoles was calculated by counting 250
801 vacuoles in three independent experiments. Data are presented as mean values ± SEM.

802 **Semi-quantitative RT-PCR.** Total mRNAs of freshly egressed extracellular parasites from the cKD
803 TgNFS2-HA, cKD TgISU1-HA and their respective complemented cell lines, as well as cKD TgISU1
804 (incubated with or without ATc at 1.5 µg/mL for 3 days) were extracted using Nucleospin RNA II Kit
805 (Macherey-Nagel). The cDNAs were synthesized with 450 ng of total RNA per RT-PCR reaction using
806 High-Capacity cDNA Reverse Transcription Kit (Applied Biosystems). Specific primers for *TgNFS2*
807 (ML4686/ML4687), *TgISU1* (ML4684/ML4685) and, as a control, *Tubulin β* (ML841/ML842) or *actin*
808 (ML843/ML844) were used to amplify specific transcripts with the GoTaq DNA polymerase
809 (Promega). PCR was performed with 21 cycles of denaturation (30 s, 95 °C), annealing (20 s, 55 °C),
810 and elongation (30 s, 72 °C).

811 **Mitochondrial membrane potential measurement.** Parasites grown for the indicated time with or
812 without ATc were mechanically released from their host cells, purified on a glass wool fiber column,
813 washed and adjusted to 10^7 parasites/ml in phenol red-free medium, and incubated in with 1.5 µM
814 of the JC-1 dye (5,5',6,6'-tetrachloro-1,1',3,3'-tetraethylbenzimidazolylcarbocyanine Iodide, T3168,
815 Invitrogen) for 30 min at 37°C, washed phenol red-free medium and analyzed by flow cytometry or
816 microscopy. Flow cytometry analysis was performed on a FACSAria III flow cytometer (Becton

817 Dickinson). An unstained control was used to define gates for analysis. 50,000 events per condition
818 were collected and data were analysed using the FlowJo Software.

819 **Quantitative label-free mass spectrometry.** Parasites of the TATi ΔKu80 and cKD TgISU1-HA cell lines
820 were grown for two days in the presence of ATc; parasites of the cKD TgNFS2-HA were grown for
821 three days in the presence of ATc. Then they were mechanically released from their host cells,
822 purified on a glass wool fiber column, washed in Hanks' Balanced Salt Solution (Gibco). Samples were
823 first normalized on parasite counts, but further adjustment was performed after parasite pellet
824 resuspension in SDS lysis buffer (50 mm Tris-HCl pH8, 10 mm EDTA pH8, 1% SDS) and protein
825 quantification with a bicinchoninic acid assay kit (Abcam). For each condition, 20 µg of total proteins
826 were separated on a 12% SDS-PAGE run for 20 min at 100 V, stained with colloidal blue (Thermo
827 Fisher Scientific), and each lane was cut in three identical fractions. Trypsin digestion and mass
828 spectrometry analysis in the Q Exactive Plus mass spectrometer (Thermo Fisher Scientific) were
829 carried out as described previously [120].

830 For peptide identification and quantification, the raw files were analyzed with MaxQuant version
831 1.6.10.43 using default settings. The minimal peptide length was set to 6. Carbamidomethylation of
832 cysteine was selected as a fixed modification and oxidation of methionine, N-terminal-
833 pyroglutamylation of glutamine and glutamate and acetylation (protein N terminus) as variable
834 modifications. Up to two missed cleavages were allowed. The files were searched against the *T.*
835 *gondii* proteome (March 2020 -https: //www.uniprot.org/proteomes/UP000005641-8450 entries).
836 Identified proteins were filtered according to the following criteria: at least two different trypsin
837 peptides with at least one unique peptide, an *E* value below 0.01 and a protein E value smaller than
838 0.01 were required. Using the above criteria, the rate of false peptide sequence assignment and false
839 protein identification were lower than 1%. Peptide ion intensity values derived from MaxQuant were
840 subjected for label-free quantitation. Unique and razor peptides were considered [121]. Statistical
841 analyses were carried out using R package software. ANOVA test with threshold of 0.05 was applied
842 to identify the significant differences in the protein abundance. Hits were retained if they were
843 quantified in at least three of the four replicates in at least one experiment. Additional candidates
844 that consistently showed absence or presence of LFQ values versus the control, and mean LFQ was
845 only considered if peptides were detected in at least three out of the four biological replicates.

846 **Statistical analysis for phenotypic assays.** Unless specified, values are usually expressed as means ±
847 standard error of the mean (SEM). Data were analysed for comparison using unpaired Student's
848 t-test with equal variance (homoscedastic) for different samples or paired Student's t-test for similar
849 samples before and after treatment. For comparisons with of ratios of groups of samples with a
850 reference set to 1, analysis of variance (ANOVA) was used.

851 **Data availability.** All raw MS data and MaxQuant files generated have been deposited to the
852 ProteomeXchange Consortium via the PRIDE partner repository
853 (https://www.ebi.ac.uk/pride/archive) with the dataset identifier PXD023854.

854

855 **Acknowledgements**

856 We are grateful to L. Sheiner, P. Bradley, B. Striepen, V. Carruthers, S. Lourido, S. Angel and D.
857 Soldati-Favre for providing cell lines, antibodies and plasmids. We thank the developers and the
858 managers of the VeupathDB.org/ToxoDB.org databases, as well as scientists who contributed
859 datasets. We also thank the MRI imaging facility for providing access to their microscopes and flow
860 cytometers, and the Mass Spectrometry Proteomics Platform (MSPP) of the BPMP laboratory. Thanks

to F. Vignols for insights into the biochemistry of Fe-S proteins. This project was supported by the Fondation pour la Recherche Médicale (Equipe FRM EQ20170336725), the Labex Parafrap (ANR-11-LABX-0024) and the Agence Nationale de la Recherche (ANR-19-CE15-0023).

Conflict of Interests

The authors declare that they have no conflict of interest.

References

1. Zimorski V, Ku C, Martin WF, Gould SB. Endosymbiotic theory for organelle origins. Current Opinion in Microbiology. 2014;22: 38–48. doi:10.1016/j.mib.2014.09.008

2. Spinelli JB, Haigis MC. The multifaceted contributions of mitochondria to cellular metabolism. Nat Cell Biol. 2018;20: 745–754. doi:10.1038/s41556-018-0124-1

3. Rolland N, Bouchnak I, Moyet L, Salvi D, Kuntz M. The main functions of plastids. In: Maréchal E, editor. Plastids. New York, NY: Springer US; 2018. pp. 73–85. doi:10.1007/978-1-4939-8654-5_5

4. Inaba T, Ito-Inaba Y. Versatile roles of plastids in plant growth and development. Plant and Cell Physiology. 2010;51: 1847–1853. doi:10.1093/pcp/pcq147

5. McFadden GI, Reith ME, Munholland J, Lang-Unnasch N. Plastid in human parasites. Nature. 1996;381: 482–482. doi:10.1038/381482a0

6. Fichera ME, Roos DS. A plastid organelle as a drug target in apicomplexan parasites. Nature. 1997;390: 407–409. doi:10.1038/37132

7. Keeling PJ. The number, speed, and impact of plastid endosymbioses in eukaryotic evolution. Annu Rev Plant Biol. 2013;64: 583–607. doi:10.1146/annurev-arplant-050312-120144

8. Gould SB, Maier U-G, Martin WF. Protein import and the origin of red complex plastids. Current Biology. 2015;25: R515–R521. doi:10.1016/j.cub.2015.04.033

9. van Dooren GG, Striepen B. The algal past and parasite present of the apicoplast. Annu Rev Microbiol. 2013;67: 271–289. doi:10.1146/annurev-micro-092412-155741

10. Sheiner L, Vaidya AB, McFadden GI. The metabolic roles of the endosymbiotic organelles of Toxoplasma and Plasmodium spp. Curr Opin Microbiol. 2013;16: 452–458. doi:10.1016/j.mib.2013.07.003

11. van Dooren GG, Hapuarachchi SV. The dark side of the chloroplast: biogenesis, metabolism and membrane biology of the apicoplast. Advances in Botanical Research. Elsevier; 2017. pp. 145–185. doi:10.1016/bs.abr.2017.06.007

12. de Souza W, Attias M, Rodrigues JCF. Particularities of mitochondrial structure in parasitic protists (Apicomplexa and Kinetoplastida). The International Journal of Biochemistry & Cell Biology. 2009;41: 2069–2080. doi:10.1016/j.biocel.2009.04.007

899 13. Ovciarikova J, Lemgruber L, Stilger KL, Sullivan WJ, Sheiner L. Mitochondrial behaviour
900 throughout the lytic cycle of Toxoplasma gondii. Sci Rep. 2017;7: 42746.
901 doi:10.1038/srep42746

902 14. Seeber F, Limenitakis J, Soldati-Favre D. Apicomplexan mitochondrial metabolism: a story of
903 gains, losses and retentions. Trends in Parasitology. 2008;24: 468–478.
904 doi:10.1016/j.pt.2008.07.004

905 15. Kobayashi T, Sato S, Takamiya S, Komaki-Yasuda K, Yano K, Hirata A, et al. Mitochondria and
906 apicoplast of Plasmodium falciparum: Behaviour on subcellular fractionation and the
907 implication. Mitochondrion. 2007;7: 125–132. doi:10.1016/j.mito.2006.11.021

908 16. Nishi M, Hu K, Murray JM, Roos DS. Organellar dynamics during the cell cycle of Toxoplasma
909 gondii. J Cell Sci. 2008;121: 1559–1568. doi:10.1242/jcs.021089

910 17. Lill R. Function and biogenesis of iron–sulphur proteins. Nature. 2009;460: 831–838.
911 doi:10.1038/nature08301

912 18. Roche B, Aussel L, Ezraty B, Mandin P, Py B, Barras F. Iron/sulfur proteins biogenesis in
913 prokaryotes: formation, regulation and diversity. Biochimica et Biophysica Acta (BBA) -
914 Bioenergetics. 2013;1827: 455–469. doi:10.1016/j.bbabio.2012.12.010

915 19. Zheng L, Cash VL, Flint DH, Dean DR. Assembly of Iron-Sulfur Clusters: identification of an
916 iscSUA-hscBA-fdx gene cluster from Azotobacter vinelandii. J Biol Chem. 1998;273: 13264–
917 13272. doi:10.1074/jbc.273.21.13264

918 20. Takahashi Y, Tokumoto U. A third bacterial system for the assembly of Iron-Sulfur clusters
919 with homologs in archaea and plastids. J Biol Chem. 2002;277: 28380–28383.
920 doi:10.1074/jbc.C200365200

921 21. Boyd ES, Thomas KM, Dai Y, Boyd JM, Outten FW. Interplay between Oxygen and Fe–S cluster
922 biogenesis: insights from the Suf pathway. Biochemistry. 2014;53: 5834–5847.
923 doi:10.1021/bi500488r

924 22. Tsaousis AD. On the origin of Iron/Sulfur cluster biosynthesis in eukaryotes. Front Microbiol.
925 2019;10: 2478. doi:10.3389/fmicb.2019.02478

926 23. Couturier J, Touraine B, Briat J-F, Gaymard F, Rouhier N. The iron-sulfur cluster assembly
927 machineries in plants: current knowledge and open questions. Front Plant Sci. 2013;4.
928 doi:10.3389/fpls.2013.00259

929 24. Lill R, Srinivasan V, Mühlenhoff U. The role of mitochondria in cytosolic-nuclear iron–sulfur
930 protein biogenesis and in cellular iron regulation. Current Opinion in Microbiology. 2014;22:
931 111–119. doi:10.1016/j.mib.2014.09.015

932 25. Aw YTV, Seidi A, Hayward JA, Lee J, Victor Makota F, Rug M, et al. A key cytosolic iron-sulfur
933 cluster synthesis protein localises to the mitochondrion of Toxoplasma gondii. Mol Microbiol.
934 2020; mmi.14651. doi:10.1111/mmi.14651

935 26. Gisselberg JE, Dellibovi-Ragheb TA, Matthews KA, Bosch G, Prigge ST. The Suf iron-sulfur
936 cluster synthesis pathway is required for apicoplast maintenance in malaria parasites. Seeber
937 F, editor. PLoS Pathog. 2013;9: e1003655. doi:10.1371/journal.ppat.1003655

938 27. Haussig JM, Matuschewski K, Kooij TWA. Identification of vital and dispensable sulfur
939 utilization factors in the Plasmodium apicoplast. Waller RF, editor. PLoS ONE. 2014;9: e89718.
940 doi:10.1371/journal.pone.0089718

941 28. Kumar B, Chaubey S, Shah P, Tanveer A, Charan M, Siddiqi MI, et al. Interaction between
942 sulphur mobilisation proteins SufB and SufC: Evidence for an iron–sulphur cluster biogenesis
943 pathway in the apicoplast of Plasmodium falciparum. International Journal for Parasitology.
944 2011;41: 991–999. doi:10.1016/j.ijpara.2011.05.006

945 29. Charan M, Singh N, Kumar B, Srivastava K, Siddiqi MI, Habib S. Sulfur mobilization for Fe-S
946 cluster assembly by the essential SUF pathway in the Plasmodium falciparum apicoplast and
947 its Inhibition. Antimicrob Agents Chemother. 2014;58: 3389–3398. doi:10.1128/AAC.02711-13

948 30. Charan M, Choudhary HH, Singh N, Sadik M, Siddiqi MI, Mishra S, et al. [Fe-S] cluster assembly
949 in the apicoplast and its indispensability in mosquito stages of the malaria parasite. FEBS J.
950 2017;284: 2629–2648. doi:10.1111/febs.14159

951 31. Pala ZR, Saxena V, Saggu GS, Garg S. Recent advances in the [Fe–S] cluster biogenesis (SUF)
952 pathway functional in the apicoplast of Plasmodium. Trends in Parasitology. 2018;34: 800–
953 809. doi:10.1016/j.pt.2018.05.010

954 32. Mazumdar J, H Wilson E, Masek K, A Hunter C, Striepen B. Apicoplast fatty acid synthesis is
955 essential for organelle biogenesis and parasite survival in Toxoplasma gondii. Proc Natl Acad
956 Sci USA. 2006;103: 13192–13197. doi:10.1073/pnas.0603391103

957 33. Nair SC, Brooks CF, Goodman CD, Sturm A, Strurm A, McFadden GI, et al. Apicoplast
958 isoprenoid precursor synthesis and the molecular basis of fosmidomycin resistance in
959 Toxoplasma gondii. J Exp Med. 2011;208: 1547–1559. doi:10.1084/jem.20110039

960 34. Bergmann A, Floyd K, Key M, Dameron C, Rees KC, Thornton LB, et al. Toxoplasma gondii
961 requires its plant-like heme biosynthesis pathway for infection. PLoS Pathog. 2020;16:
962 e1008499. doi:10.1371/journal.ppat.1008499

963 35. Tjhin ET, Hayward JA, McFadden GI, van Dooren GG. Characterization of the apicoplast-
964 localized enzyme TgUroD in Toxoplasma gondii reveals a key role of the apicoplast in heme
965 biosynthesis. J Biol Chem. 2020;295: 1539–1550. doi:10.1074/jbc.RA119.011605

966 36. Harb OS, Roos DS. ToxoDB: functional genomics resource for Toxoplasma and related
967 organisms. Methods Mol Biol. 2020;2071: 27–47. doi:10.1007/978-1-4939-9857-9_2

968 37. Barylyuk K, Koreny L, Ke H, Butterworth S, Crook OM, Lassadi I, et al. A comprehensive
969 subcellular atlas of the Toxoplasma proteome via hyperLOPIT provides spatial context for
970 protein functions. Cell Host & Microbe. 2020; S193131282030514X.
971 doi:10.1016/j.chom.2020.09.011

972 38. Sidik SM, Huet D, Ganesan SM, Huynh M-H, Wang T, Nasamu AS, et al. A Genome-wide CRISPR
973 Screen in Toxoplasma Identifies Essential Apicomplexan Genes. Cell. 2016;166: 1423-
974 1435.e12. doi:10.1016/j.cell.2016.08.019

975 39. Braymer JJ, Freibert SA, Rakwalska-Bange M, Lill R. Mechanistic concepts of iron-sulfur protein
976 biogenesis in Biology. Biochimica et Biophysica Acta (BBA) - Molecular Cell Research.
977 2021;1868: 118863. doi:10.1016/j.bbamcr.2020.118863

978 40. Outten FW, Djaman O, Storz G. A suf operon requirement for Fe-S cluster assembly during
979 iron starvation in Escherichia coli: suf operon role during iron starvation. Molecular
980 Microbiology. 2004;52: 861–872. doi:10.1111/j.1365-2958.2004.04025.x

981 41. Fox BA, Ristuccia JG, Gigley JP, Bzik DJ. Efficient gene replacements in Toxoplasma gondii
982 strains deficient for nonhomologous end joining. Eukaryotic Cell. 2009;8: 520–529.
983 doi:10.1128/EC.00357-08

984 42. Huynh M-H, Carruthers VB. Tagging of endogenous genes in a Toxoplasma gondii strain
985 lacking Ku80. Eukaryot Cell. 2009;8: 530–539. doi:10.1128/EC.00358-08

986 43. Sheiner L, Demerly JL, Poulsen N, Beatty WL, Lucas O, Behnke MS, et al. A Systematic Screen
987 to Discover and Analyze Apicoplast Proteins Identifies a Conserved and Essential Protein
988 Import Factor. PLoS Pathog. 2011;7. doi:10.1371/journal.ppat.1002392

989 44. Pino P, Foth BJ, Kwok L-Y, Sheiner L, Schepers R, Soldati T, et al. Dual targeting of antioxidant
990 and metabolic enzymes to the mitochondrion and the apicoplast of Toxoplasma gondii. PLoS
991 Pathog. 2007;3: e115. doi:10.1371/journal.ppat.0030115

992 45. Ollagnier-de-Choudens S, Lascoux D, Loiseau L, Barras F, Forest E, Fontecave M. Mechanistic
993 studies of the SufS-SufE cysteine desulfurase: evidence for sulfur transfer from SufS to SufE.
994 FEBS Lett. 2003;555: 263–267. doi:10.1016/s0014-5793(03)01244-4

995 46. Narayana Murthy, UM, Ollagnier-de-Choudens S, Sanakis Y, Abdel-Ghany SE, Rousset C, Ye H,
996 et al. Characterization of Arabidopsis thaliana SufE2 and SufE3: functions in chloroplast iron-
997 sulfur cluster assembly and NAD synthesis. J Biol Chem. 2007;282: 18254–18264.
998 doi:10.1074/jbc.M701428200

999 47. Meissner M, Brecht S, Bujard H, Soldati D. Modulation of myosin A expression by a newly
1000 established tetracycline repressor-based inducible system in Toxoplasma gondii. Nucleic Acids
1001 Res. 2001;29: E115.

1002 48. Jelenska J, Crawford MJ, Harb OS, Zuther E, Haselkorn R, Roos DS, et al. Subcellular localization
1003 of acetyl-CoA carboxylase in the apicomplexan parasite Toxoplasma gondii. Proceedings of the
1004 National Academy of Sciences. 2001;98: 2723–2728. doi:10.1073/pnas.051629998

1005 49. Pfefferkorn ER, Nothnagel RF, Borotz SE. Parasiticidal effect of clindamycin on Toxoplasma
1006 gondii grown in cultured cells and selection of a drug-resistant mutant. Antimicrob Agents
1007 Chemother. 1992;36: 1091–1096.

1008 50. He CY, Shaw MK, Pletcher CH, Striepen B, Tilney LG, Roos DS. A plastid segregation defect in
1009 the protozoan parasite Toxoplasma gondii. EMBO J. 2001;20: 330–339.
1010 doi:10.1093/emboj/20.3.330

1011 51. Blader IJ, Coleman BI, Chen C-T, Gubbels M-J. Lytic cycle of Toxoplasma gondii: 15 years later.
1012 Annu Rev Microbiol. 2015;69: 463–485. doi:10.1146/annurev-micro-091014-104100

1013 52. Dubey JP, Lindsay DS, Speer CA. Structures of Toxoplasma gondii tachyzoites, bradyzoites, and
1014 sporozoites and biology and development of tissue cysts. Clin Microbiol Rev. 1998;11: 267–
1015 299.

1016 53. Cerutti A, Blanchard N, Besteiro S. The bradyzoite: a key developmental stage for the
1017 persistence and pathogenesis of toxoplasmosis. Pathogens. 2020;9.
1018 doi:10.3390/pathogens9030234

1019 54. Sibley LD, Boothroyd JC. Virulent strains of Toxoplasma gondii comprise a single clonal lineage.
1020 Nature. 1992;359: 82–85. doi:10.1038/359082a0

1021 55. Valasatava Y, Rosato A, Banci L, Andreini C. MetalPredator: a web server to predict iron-sulfur
1022 cluster binding proteomes. Bioinformatics. 2016;32: 2850–2852.
1023 doi:10.1093/bioinformatics/btw238

1024 56. Fuss JO, Tsai C-L, Ishida JP, Tainer JA. Emerging critical roles of Fe–S clusters in DNA replication
1025 and repair. Biochimica et Biophysica Acta (BBA) - Molecular Cell Research. 2015;1853: 1253–
1026 1271. doi:10.1016/j.bbamcr.2015.01.018

1027 57. Thomsen-Zieger N, Schachtner J, Seeber F. Apicomplexan parasites contain a single lipoic acid
1028 synthase located in the plastid. FEBS Lett. 2003;547: 80–86. doi:10.1016/s0014-
1029 5793(03)00673-2

1030 58. Pierrel F, Douki T, Fontecave M, Atta M. MiaB protein is a bifunctional radical-S-
1031 adenosylmethionine enzyme involved in thiolation and methylation of tRNA. J Biol Chem.
1032 2004;279: 47555–47563. doi:10.1074/jbc.M408562200

1033 59. Imlay L, Odom AR. Isoprenoid metabolism in apicomplexan parasites. Curr Clin Microbiol Rep.
1034 2014;1: 37–50. doi:10.1007/s40588-014-0006-7

1035 60. Seidi A, Muellner-Wong LS, Rajendran E, Tjhin ET, Dagley LF, Aw VY, et al. Elucidating the
1036 mitochondrial proteome of Toxoplasma gondii reveals the presence of a divergent
1037 cytochrome c oxidase. Elife. 2018;7. doi:10.7554/eLife.38131

1038 61. Hayward JA, Rajendran E, Zwahlen SM, Faou P, van Dooren GG. Divergent features of the
1039 coenzyme Q:cytochrome c oxidoreductase complex in Toxoplasma gondii parasites. PLoS
1040 Pathog. 2021;17: e1009211. doi:10.1371/journal.ppat.1009211

1041 62. Maclean AE, Bridges HR, Silva MF, Ding S, Ovciarikova J, Hirst J, et al. Complexome profile of
1042 Toxoplasma gondii mitochondria identifies divergent subunits of respiratory chain complexes
1043 including new subunits of cytochrome bc1 complex. PLoS Pathog. 2021;17: e1009301.
1044 doi:10.1371/journal.ppat.1009301

1045 63. Lanz ND, Booker SJ. Auxiliary iron–sulfur cofactors in radical SAM enzymes. Biochimica et
1046 Biophysica Acta (BBA) - Molecular Cell Research. 2015;1853: 1316–1334.
1047 doi:10.1016/j.bbamcr.2015.01.002

1048 64. Pittman KJ, Aliota MT, Knoll LJ. Dual transcriptional profiling of mice and Toxoplasma gondii
1049 during acute and chronic infection. BMC Genomics. 2014;15: 806. doi:10.1186/1471-2164-15-
1050 806

1051 65. Hehl AB, Basso WU, Lippuner C, Ramakrishnan C, Okoniewski M, Walker RA, et al. Asexual
1052 expansion of Toxoplasma gondii merozoites is distinct from tachyzoites and entails expression
1053 of non-overlapping gene families to attach, invade, and replicate within feline enterocytes.
1054 BMC Genomics. 2015;16: 66. doi:10.1186/s12864-015-1225-x

1055 66. Jung C, Lee CY-F, Grigg ME. The SRS superfamily of Toxoplasma surface proteins. International
1056 Journal for Parasitology. 2004;34: 285–296. doi:10.1016/j.ijpara.2003.12.004

1057 67. Li L, Brunk BP, Kissinger JC, Pape D, Tang K, Cole RH, et al. Gene discovery in the apicomplexa
1058 as revealed by EST sequencing and assembly of a comparative gene database. Genome Res.
1059 2003;13: 443–454. doi:10.1101/gr.693203

1060 68. Tomita T, Bzik DJ, Ma YF, Fox BA, Markillie LM, Taylor RC, et al. The Toxoplasma gondii cyst
1061 wall protein CST1 is critical for cyst wall integrity and promotes bradyzoite persistence. PLoS
1062 Pathog. 2013;9: e1003823. doi:10.1371/journal.ppat.1003823

1063 69. Yang J, Zhang L, Diao H, Xia N, Zhou Y, Zhao J, et al. ANK1 and DnaK-TPR, two tetratricopeptide
1064 repeat-containing proteins primarily expressed in Toxoplasma bradyzoites, do not contribute
1065 to bradyzoite differentiation. Front Microbiol. 2017;8: 2210. doi:10.3389/fmicb.2017.02210

1066 70. Nadipuram SM, Thind AC, Rayatpisheh S, Wohlschlegel JA, Bradley PJ. Proximity biotinylation
1067 reveals novel secreted dense granule proteins of Toxoplasma gondii bradyzoites. PLoS One.
1068 2020;15: e0232552. doi:10.1371/journal.pone.0232552

1069 71. Huet D, Rajendran E, van Dooren GG, Lourido S. Identification of cryptic subunits from an
1070 apicomplexan ATP synthase. eLife. 2018;7: e38097. doi:10.7554/eLife.38097

1071 72. Bohne W, Heesemann J, Gross U. Reduced replication of Toxoplasma gondii is necessary for
1072 induction of bradyzoite-specific antigens: a possible role for nitric oxide in triggering stage
1073 conversion. Infect Immun. 1994;62: 1761–1767.

1074 73. Crack JC, Green J, Thomson AJ, Le Brun NE. Iron-sulfur clusters as biological sensors: the
1075 chemistry of reactions with molecular oxygen and nitric oxide. Acc Chem Res. 2014;47: 3196–
1076 3205. doi:10.1021/ar5002507

1077 74. Soete M, Fortier B, Camus D, Dubremetz JF. Toxoplasma gondii: kinetics of bradyzoite-
1078 tachyzoite interconversion in vitro. Exp Parasitol. 1993;76: 259–264.
1079 doi:10.1006/expr.1993.1031

1080 75. Lacombe A, Maclean AE, Ovciarikova J, Tottey J, Mühleip A, Fernandes P, et al. Identification
1081 of the Toxoplasma gondii mitochondrial ribosome, and characterisation of a protein essential
1082 for mitochondrial translation. Mol Microbiol. 2019;112: 1235–1252. doi:10.1111/mmi.14357

1083 76. Tomavo S, Boothroyd JC. Interconnection between organellar functions, development and
1084 drug resistance in the protozoan parasite, Toxoplasma gondii. International Journal for
1085 Parasitology. 1995;25: 1293–1299. doi:10.1016/0020-7519(95)00066-B

1086 77. Biddau M, Sheiner L. Targeting the apicoplast in malaria. Biochem Soc Trans. 2019;47: 973–
1087 983. doi:10.1042/BST20170563

1088 78. Mather MW, Henry KW, Vaidya AB. Mitochondrial drug targets in apicomplexan parasites.
1089 Curr Drug Targets. 2007;8: 49–60. doi:10.2174/138945007779315632

1090 79. Dunay IR, Gajurel K, Dhakal R, Liesenfeld O, Montoya JG. Treatment of toxoplasmosis:
1091 historical perspective, animal models, and current clinical practice. Clin Microbiol Reviews.
1092 2018;31: e00057-17, /cmr/31/4/e00057-17.atom. doi:10.1128/CMR.00057-17

1093 80. Goodman CD, Pasaje CFA, Kennedy K, McFadden GI, Ralph SA. Targeting protein translation in
1094 organelles of the Apicomplexa. Trends in Parasitology. 2016;32: 953–965.
1095 doi:10.1016/j.pt.2016.09.011

1096 81. Baggish AL, Hill DR. Antiparasitic agent atovaquone. Antimicrob Agents Chemother. 2002;46:
1097 1163–1173. doi:10.1128/aac.46.5.1163-1173.2002

1098 82. Gross U, Pohl F. Influence of antimicrobial agents on replication and stage conversion of
1099 Toxoplasma gondii. Curr Top Microbiol Immunol. 1996;219: 235–245. doi:10.1007/978-3-642-
1100 51014-4_21

1101 83. Kennedy K, Crisafulli EM, Ralph SA. Delayed death by plastid inhibition in apicomplexan
1102 parasites. Trends in Parasitology. 2019;35: 747–759. doi:10.1016/j.pt.2019.07.010

1103 84. Kawamukai M. Biosynthesis of coenzyme Q in eukaryotes. Bioscience, Biotechnology, and
1104 Biochemistry. 2016;80: 23–33. doi:10.1080/09168451.2015.1065172

1105 85. Liang X, Cui J, Yang X, Xia N, Li Y, Zhao J, et al. Acquisition of exogenous fatty acids renders
1106 apicoplast-based biosynthesis dispensable in tachyzoites of Toxoplasma. J Biol Chem.
1107 2020;295: 7743–7752. doi:10.1074/jbc.RA120.013004

1108 86. Amiar S, MacRae JI, Callahan DL, Dubois D, van Dooren GG, Shears MJ, et al. Apicoplast-
1109 localized lysophosphatidic acid precursor assembly is required for bulk phospholipid synthesis
1110 in Toxoplasma gondii and relies on an algal/plant-like glycerol 3-phosphate acyltransferase.
1111 PLOS Pathogens. 2016;12: e1005765. doi:10.1371/journal.ppat.1005765

1112 87. Amiar S, Katris NJ, Berry L, Dass S, Duley S, Arnold C-S, et al. Division and adaptation to host
1113 environment of apicomplexan parasites depend on apicoplast lipid metabolic plasticity and
1114 host organelle remodeling. Cell Reports. 2020;30: 3778-3792.e9.
1115 doi:10.1016/j.celrep.2020.02.072

1116 88. Martins-Duarte ÉS, Carias M, Vommaro R, Surolia N, de Souza W. Apicoplast fatty acid
1117 synthesis is essential for pellicle formation at the end of cytokinesis in Toxoplasma gondii. J
1118 Cell Sci. 2016;129: 3320–3331. doi:10.1242/jcs.185223

1119 89. Ramakrishnan S, Docampo MD, Macrae JI, Pujol FM, Brooks CF, van Dooren GG, et al.
1120 Apicoplast and endoplasmic reticulum cooperate in fatty acid biosynthesis in apicomplexan
1121 parasite Toxoplasma gondii. J Biol Chem. 2012;287: 4957–4971.
1122 doi:10.1074/jbc.M111.310144

1123 90. Dubois D, Fernandes S, Amiar S, Dass S, Katris NJ, Botté CY, et al. Toxoplasma gondii acetyl-
1124 CoA synthetase is involved in fatty acid elongation (of long fatty acid chains) during tachyzoite
1125 life stages. J Lipid Res. 2018;59: 994–1004. doi:10.1194/jlr.M082891

1126 91. MacRae JI, Sheiner L, Nahid A, Tonkin C, Striepen B, McConville MJ. Mitochondrial metabolism
1127 of glucose and glutamine is required for intracellular growth of Toxoplasma gondii. Cell Host
1128 Microbe. 2012;12: 682–692. doi:10.1016/j.chom.2012.09.013

1129 92. Shukla A, Olszewski KL, Llinás M, Rommereim LM, Fox BA, Bzik DJ, et al. Glycolysis is important
1130 for optimal asexual growth and formation of mature tissue cysts by Toxoplasma gondii.
1131 International Journal for Parasitology. 2018;48: 955–968. doi:10.1016/j.ijpara.2018.05.013

1132 93. Denton H, Roberts CW, Alexander J, Thong KW, Coombs GH. Enzymes of energy metabolism in
1133 the bradyzoites and tachyzoites of Toxoplasma gondii. FEMS Microbiol Lett. 1996;137: 103–
1134 108. doi:10.1111/j.1574-6968.1996.tb08090.x

1135 94. Dzierszinski F, Nishi M, Ouko L, Roos DS. Dynamics of Toxoplasma gondii differentiation.
1136 Eukaryotic Cell. 2004;3: 992–1003. doi:10.1128/EC.3.4.992-1003.2004

1137 95. Watts E, Zhao Y, Dhara A, Eller B, Patwardhan A, Sinai AP. Novel Approaches Reveal that
1138 Toxoplasma gondii Bradyzoites within Tissue Cysts Are Dynamic and Replicating Entities In
1139 Vivo. MBio. 2015;6: e01155-01115. doi:10.1128/mBio.01155-15

1140 96. McHugh TD, Holliman RE, Butcher PD. The in vitro model of tissue cyst formation in
1141 Toxoplasma gondii. Parasitology Today. 1994;10: 281–285. doi:10.1016/0169-4758(94)90148-
1142 1

1143 97. Chandel NS. Evolution of mitochondria as signaling organelles. Cell Metab. 2015;22: 204–206.
1144 doi:10.1016/j.cmet.2015.05.013

1145 98. Martínez-Reyes I, Diebold LP, Kong H, Schieber M, Huang H, Hensley CT, et al. TCA cycle and
1146 mitochondrial membrane potential are necessary for diverse biological functions. Mol Cell.
1147 2016;61: 199–209. doi:10.1016/j.molcel.2015.12.002

1148 99. Sagot I, Laporte D. The cell biology of quiescent yeast – a diversity of individual scenarios. J
1149 Cell Sci. 2019;132: jcs213025. doi:10.1242/jcs.213025

1150 100. Yalamanchili N, Kriete A, Alfego D, Danowski KM, Kari C, Rodeck U. Distinct cell stress
1151 responses induced by ATP restriction in quiescent human fibroblasts. Front Genet. 2016;7:
1152 171. doi:10.3389/fgene.2016.00171

1153 101. Waldman BS, Schwarz D, Wadsworth MH, Saeij JP, Shalek AK, Lourido S. Identification of a
1154 master regulator of differentiation in Toxoplasma. Cell. 2020; S0092867419313753.
1155 doi:10.1016/j.cell.2019.12.013

1156 102. Hassan MA, Vasquez JJ, Guo-Liang C, Meissner M, Nicolai Siegel T. Comparative ribosome
1157 profiling uncovers a dominant role for translational control in Toxoplasma gondii. BMC
1158 Genomics. 2017;18: 961. doi:10.1186/s12864-017-4362-6

1159 103. Holmes MJ, Augusto L da S, Zhang M, Wek RC, Sullivan WJ. Translational control in the latency
1160 of apicomplexan parasites. Trends in Parasitology. 2017;33: 947–960.
1161 doi:10.1016/j.pt.2017.08.006

1162 104. Harvey R, Dezi V, Pizzinga M, Willis AE. Post-transcriptional control of gene expression
1163 following stress: the role of RNA-binding proteins. Biochem Soc Trans. 2017;45: 1007–1014.
1164 doi:10.1042/BST20160364

1165 105. Lirussi D, Matrajt M. RNA granules present only in extracellular Toxoplasma gondii increase
1166 parasite viability. Int J Biol Sci. 2011;7: 960–967. doi:10.7150/ijbs.7.960

1167 106. Liu M, Miao J, Liu T, Sullivan WJ, Cui L, Chen X. Characterization of TgPuf1, a member of the
1168 Puf family RNA-binding proteins from Toxoplasma gondii. Parasit Vectors. 2014;7: 141.
1169 doi:10.1186/1756-3305-7-141

1170 107. Gissot M, Walker R, Delhaye S, Alayi TD, Huot L, Hot D, et al. Toxoplasma gondii Alba proteins
1171 are involved in translational control of gene expression. J Mol Biol. 2013;425: 1287–1301.
1172 doi:10.1016/j.jmb.2013.01.039

1173 108. Gastens MH, Fischer H-G. Toxoplasma gondii eukaryotic translation initiation factor 4A
1174 associated with tachyzoite virulence is down-regulated in the bradyzoite stage. Int J Parasitol.
1175 2002;32: 1225–1234. doi:10.1016/s0020-7519(02)00096-6

1176 109. Balk J, Pilon M. Ancient and essential: the assembly of iron–sulfur clusters in plants. Trends in
1177 Plant Science. 2011;16: 218–226. doi:10.1016/j.tplants.2010.12.006

1178 110. Shanmugasundram A, Gonzalez-Galarza FF, Wastling JM, Vasieva O, Jones AR. Library of
1179 Apicomplexan Metabolic Pathways: a manually curated database for metabolic pathways of
1180 apicomplexan parasites. Nucleic Acids Research. 2013;41: D706–D713.
1181 doi:10.1093/nar/gks1139

1182 111. Morlon-Guyot J, Berry L, Chen C-T, Gubbels M-J, Lebrun M, Daher W. The Toxoplasma gondii
1183 calcium-dependent protein kinase 7 is involved in early steps of parasite division and is crucial
1184 for parasite survival. Cell Microbiol. 2014;16: 95–114. doi:10.1111/cmi.12186

1185 112. Couvreur G, Sadak A, Fortier B, Dubremetz JF. Surface antigens of Toxoplasma gondii.
1186 Parasitology. 1988;97 (Pt 1): 1–10.

1187 113. Agrawal S, van Dooren GG, Beatty WL, Striepen B. Genetic evidence that an endosymbiont-
1188 derived endoplasmic reticulum-associated protein degradation (ERAD) system functions in
1189 import of apicoplast proteins. J Biol Chem. 2009;284: 33683–33691.
1190 doi:10.1074/jbc.M109.044024

1191 114. Herm-Gotz A. Toxoplasma gondii myosin A and its light chain: a fast, single-headed, plus-end-
1192 directed motor. The EMBO Journal. 2002;21: 2149–2158. doi:10.1093/emboj/21.9.2149

1193 115. Bermudes D, Dubremetz J-F, Achbarou A, Joiner KA. Cloning of a cDNA encoding the dense
1194 granule protein GRA3 from Toxoplasma gondii. Molecular and Biochemical Parasitology.
1195 1994;68: 247–257. doi:10.1016/0166-6851(94)90169-4

1196 116. de Miguel N, Echeverria PC, Angel SO. Differential subcellular localization of members of the
1197 Toxoplasma gondii small heat shock protein family. Eukaryot Cell. 2005;4: 1990–1997.
1198 doi:10.1128/EC.4.12.1990-1997.2005

1199 117. Plattner F, Yarovinsky F, Romero S, Didry D, Carlier M-F, Sher A, et al. Toxoplasma profilin is
1200 essential for host cell invasion and TLR11-dependent induction of an interleukin-12 response.
1201 Cell Host Microbe. 2008;3: 77–87. doi:10.1016/j.chom.2008.01.001

1202 118. Tomavo S, Fortier B, Soete M, Ansel C, Camus D, Dubremetz JF. Characterization of
1203 bradyzoite-specific antigens of Toxoplasma gondii. Infect Immun. 1991;59: 3750–3753.
1204 doi:10.1128/IAI.59.10.3750-3753.1991

1205 119. Jia Y, Marq J-B, Bisio H, Jacot D, Mueller C, Yu L, et al. Crosstalk between PKA and PKG controls
1206 pH-dependent host cell egress of Toxoplasma gondii. EMBO J. 2017;36: 3250–3267.
1207 doi:10.15252/embj.201796794

1208 120. Berger N, Vignols F, Przybyla-Toscano J, Roland M, Rofidal V, Touraine B, et al. Identification of
1209 client iron–sulfur proteins of the chloroplastic NFU2 transfer protein in Arabidopsis thaliana.

1210 Takahashi H, editor. Journal of Experimental Botany. 2020;71: 4171–4187.
1211 doi:10.1093/jxb/eraa166

1212 121. Cox J, Mann M. MaxQuant enables high peptide identification rates, individualized p.p.b.-
1213 range mass accuracies and proteome-wide protein quantification. Nat Biotechnol. 2008;26:
1214 1367–1372. doi:10.1038/nbt.1511

1215 **Figure legends**
1216
1217 **Figure 1. TgNFS2 and TgISU1 are functional homologs of components of iron-sulfur cluster**
1218 **synthesis pathways.**
1219 A) Putative Fe-S cluster synthesis pathways and associated molecular machinery in *Toxoplasma*. B)
1220 Functional complementation of bacterial mutants for IscU (top) and SufS (bottom). Growth of 'wild-
1221 type' (WT) *E. coli* K12 parental strain, bacterial mutant strains and strains complemented ('comp') by
1222 their respective *T. gondii* homologues ('comp'), was assessed by monitoring the optical density at
1223 600 nm in the presence or not of an iron chelator (2,2'-bipyridyl, 'chel'). Values are mean from n=3
1224 independent experiments ±SEM. * denotes $p \leq 0.05$, Student's t-test.
1225
1226
1227 **Figure 2. TgNFS2 and TgISU1 localize to the apicoplast and the mitochondrion, respectively.**
1228 Detection by immunoblot of C-terminally HA-tagged TgNFS2 (A) and TgISU1 (B) in parasite extracts
1229 reveals the presence of both precusor (p) and mature (m) forms of the proteins. Anti-actin (TgACT1)
1230 antibody was used as a loading control. Immunofluorescence assay shows TgNFS2 co-localizes with
1231 apicoplast marker TgCPN60 (C) and TgISU1 co-localizes with mitochondrial marker F1 β ATPase (D).
1232 Scale bar represents 5 µm. DNA was labelled with DAPI. DIC: differential interference contrast.
1233
1234 **Figure 3. Efficient down-regulation of TgNFS2 and TgISU1 expression with anhydrotetracyclin (ATc).**
1235 A) Immunoblot analysis with anti-HA antibody shows efficient down-regulation of TgNFS2 after 48h
1236 of incubation with ATc. Anti-SAG1 antibody was used as a loading control. B) Immunoblot analysis
1237 with anti-HA antibody shows efficient down-regulation of TgISU1 after 24h of incubation with ATc.
1238 Anti-SAG1 antibody was used as a loading control. C) and D) Immunofluorescence assays show
1239 TgNFS2 and TgISU1 are not detectable anymore after 48h of incubation with ATc. Scale bar
1240 represents 5 µm. DNA was labelled with DAPI. DIC: differential interference contrast.
1241
1242 **Figure 4. Depletion of TgNFS2 or TgISU1 affects in vitro growth of the tachyzoites.** Plaque assays
1243 were carried out by infecting HFF monolayers with the TATi ΔKu80 cell line, the cKD TgNFS2-HA (A) or
1244 the cKD TgISU1-HA (B) cell lines, or parasites complemented with a wild-type version of the
1245 respective proteins. They were grown for 7 days ± ATc. Measurements of lysis plaque areas are
1246 shown on the right and highlight a significant defect in the lytic cycle when TgNFS2 (A) or TgISU1 (B)
1247 were depleted. Values are means of n=3 experiments ± SEM. Mean value of TATi ΔKu80 control was
1248 set to 100% as a reference. **** denotes $p \leq 0.0001$, Student's t-test. Scale bars= 1mm. TgNFS2 (C)
1249 and TgISU1 (D) mutant and complemented cell lines, as well as their parental cell lines and the TATi
1250 ΔKu80 control, were grown in HFF in the presence or absence of ATc for 48 hours, and subsequently
1251 allowed to invade and grow in new HFF cells for an extra 24 hours in the presence of ATc. Parasites
1252 per vacuole were then counted. Values are means ± SEM from n=3 independent experiments for
1253 which 200 vacuoles were counted for each condition. **E**) Plaque assays for the TgNFS2 and TgISU1
1254 mutants were performed as described in A) and B), but ATc was washed out after 7 days (7 days+ 7
1255 days-) or not (14 days+), and parasites were left to grow for an extra 7 days. Plaque area was
1256 measured. Data are means ± SEM from three independent experiments. *** $p \leq 0.001$, Student's
1257 t-test. Arrowheads show plaques forming in the TgISU1 upon ATc removal. Scale bar= 1mm.

1258

1259 **Figure 5. Impact of TgNFS2 and TgISU1 depletion on intracellular tachyzoites.**
1260 A) Depletion of TgNFS2 impacts the apicoplast. cKD TgNFS2-HA parasites were kept in the presence
1261 of ATc and the aspect of the apicoplast and mitochondrion was evaluated by microscopic observation
1262 using specific markers (CPN60 and F1β ATPase, respectively). After 72 hours, parasites egressed and
1263 were used to reinvade new host cells for subsequent timepoints. Scale bar represents 5 µm. DNA was
1264 labelled with DAPI. DIC: differential interference contrast. B) Quantification of apicoplast loss in
1265 vacuoles containing cKD TgNFS2-HA parasites after 72 to 120 hours of incubation with ATc. Data are
1266 mean values from *n*=3 independent experiments ±SEM. ** $p \leq 0.01$, **** $p \leq 0.0001$, Student's *t*-test.
1267 C) Depletion of TgISU1 does not impact mitochondrial and overall parasite morphologies, but affects
1268 parasite growth. cKD TgISU1-HA parasites were grown in the presence of ATc for up to five days and
1269 the aspect of the apicoplast and mitochondrion was evaluated by microscopic observation using
1270 specific markers described in A). Growth in the presence of ATc was continuous for up to five days.
1271 Scale bar represents 5 µm. DNA was labelled with DAPI. DIC: differential interference contrast. D)
1272 Egress is not affected by TgISU1depletion. An egress assay was performed using calcium ionophore
1273 A23187. On the left are representative images of vacuoles containing parasites that egressed
1274 normally or did not. GRA3 (parasitophorous vacuole marker) staining is shown in green and GAP45
1275 (parasite periphery marker) in red. Scale bars= 10µm. On the right is the quantification of egress for
1276 cKD TgISU1-HA parasites kept in the presence of ATc or not. Mean values ± SEM from *n*=3
1277 independent biological experiments are represented.
1278

1279 **Figure 6. Change in protein expression induced by TgNFS2 and TgISU1 depletion.** Volcano plots
1280 showing the protein expression difference based on label-free quantitative proteomic data from
1281 TgNFS2 (A) and TgISU1 (B) mutants grown in the presence of ATc. X-axis shows log2 fold change
1282 versus the TATi ΔKu80 control grown in the same conditions, and the Y-axis shows -log10(p value)
1283 after ANOVA statistical test for *n*=4 independent biological replicates. Selected variant protein
1284 categories are highlighted in color. C) Venn diagram representation of the shared and unique
1285 proteins whose expression is affected by the depletion of TgNFS2 and TgISU1. D) and E): mapping of
1286 less or more abundant candidates in the TgNFS2 and TgISU1 mutants, respectively, on the spatial
1287 proteome map representation of the hyperLOPIT data highlighting clusters denoting putative
1288 subcellular localization. Full details available at: https://proteome.shinyapps.io/toxolopittzex/.

1289

1290 **Figure 7. TgNFS2 depletion impacts apicoplast-related pathways and has deleterious effects on**
1291 **parasite replication.** A) A decrease in the lipoylation of the E2 subunit of pyruvate dehydrogenase
1292 (TgPDH-E2), which depends on the Fe-S-containing lipoyl synthase called LipA in the apicoplast, was
1293 observed by immunoblot using an anti-lipoic acid antibody on cell extracts from cKD TgNFS2-HA
1294 parasites kept with ATc for an increasing period of time. TgCPN60 was used as a control for
1295 apicoplast integrity. TgSAG1 was used as a loading control. Decrease of lipoylated TgPDH-E2 was
1296 quantified by band densitometry and normalized with the internal loading control. Data represented
1297 are mean ±SEM of *n*=3 independent experiments. ** $p \leq 0.01$, *** $p \leq 0.001$ ANOVA comparison. B)
1298 cKD TgNFS2-HA parasites that were grown in the presence of ATc for 5 days were co-stained with
1299 anti-TgIMC3 (to outline parasites and internal buds) and anti-CPN60 (an apicoplast marker), which
1300 highlighted abnormal membrane structures and organelle segregation problems. Scale bar
1301 represents 5 µm. DNA was labelled with DAPI. DIC: differential interference contrast.
1302

1303 **Figure 8. TgISU1 depletion impacts the mitochondrial respiratory chain.** A) Schematic
1304 representation of the *T. gondii* mitochondrial respiratory chain; listed are the subunits of the
1305 different complexes that were found less abundant upon TgISU1 depletion; Fe-S proteins are
1306 highlighted in green. SDH: succinate dehydrogenase; CoQ: coenzyme Q B) Immunofluorescence
1307 analysis of cKD TgISU1 parasites expressing HA-tagged TgSDHB (top) or TgApiCox13 (bottom)

1308 showing a decrease in expression in the HA-tagged candidates after 3 days of incubation with ATc.
1309 Images were taken with the same exposure time for similar channels. TgHSP29 was used as a
1310 mitochondrial marker. Scale bar represents 10 µm. DNA was labelled with DAPI. C) Immunoblot
1311 analysis of TgSDHB (top) and TgApiCox13 (bottom) levels upon depletion of TgISU1 after 3 days of
1312 incubation with ATc. TgACT1 was used as a loading control. Protein levels were quantified by band
1313 densitometry and normalized with the internal loading control. Data represented are mean ±SEM of
1314 *n*=5 independent experiments. ** $p \leq 0.01$, *** $p \leq 0.001$, ANOVA comparison. D) Impact of TgISU1
1315 depletion on the parasite mitochondrial membrane potential was measured by JC-1 labelling. cKD
1316 TgISU1-HA parasites were grown or not in the presence of ATc, mechanically released from their host
1317 cells and labelled with the JC-1 dye. This dye exhibits potential-dependent accumulation in the
1318 mitochondrion, indicated by a switch from green fluorescence for the monomeric form of the probe,
1319 to a concentration-dependent formation of red aggregates (inset, DNA is labelled with DAPI and
1320 shown in blue, scale=1µm). Parasites were then analysed by flow cytometry. Unlabelled parasites (no
1321 JC-1) was used as a control for gating. Numbers represent the percentage of cells in each of the
1322 subpopulations (P1, P2, P3). One representative experiment out of *n*=3 biological replicates is shown.
1323
1324 **Figure 9. Depletion of TgISU1 triggers parasite differentiation.**
1325 A) cKD TgISU1-HA parasites were grown in the presence of ATc and labelled with anti-TgIMC3 (to
1326 outline parasites) and a lectin of *Dolicos biflorus* (DBL) to specifically outline nascent cyst walls. Scale
1327 bar represents 10 µm. DNA was labelled with DAPI. DIC: differential interference contrast. B)
1328 Quantification of DBL-positive vacuoles after 24 hours or 48 hours of culture of 1) the cKD TgISU1-HA
1329 and cKD TgNFS2-HA mutants in the presence or absence of ATc 2) the Tati ΔKu80 cell line, as a
1330 negative control, 3) the Tati ΔKu80 cell line in the presence of 100µM nitric oxide (NO), as a positive
1331 control. Data are from *n*=3 independent experiments. Values are mean ±SEM. * $p \leq 0.05$, ** $p \leq 0.01$,
1332 Student's *t*-test C) Clustering of bradyzoite (Bz) or tachyzoite (Tz)-specific proteins of the SRS family
1333 shows specific enrichment of bradyzoite proteins upon TgISU1 depletion. D) The cKD TgISU1-HA
1334 mutant was grown for up to 14 days in the presence of ATc and labelled for tachyzoite marker SAG1,
1335 or intermediate (P18/SAG4) or late (P21) bradyzoite markers. Scale bar represents 10 µm. DNA was
1336 labelled with DAPI. DIC: differential interference contrast. E) Measurement of the cyst area size after
1337 growing the cKD TgISU1-HA mutant for 7 and 14 days in the presence of ATc and labelling the cyst
1338 wall with DBL and measuring the surface of 60 cysts per condition. Mean ±SD is represented. One
1339 representative experiment out of three independent biological replicates is shown. **** denotes $p \leq$
1340 0.0001, Student's *t*-test.
1341
1342 **Figure 10. Other mitochondrial mutants remain viable and initiate stage conversion.** A) Plaque
1343 assays for the TgQCR11 and TgmS35 mutants were performed by infecting HFF monolayers with cKD
1344 cell lines and letting them grow in absence (7 days -) or presence of ATc (7 days +), after 7 days ATc
1345 was washed out (7 days+ 7days-) or not (14 days+), and parasites were left to grow for an extra 7
1346 days. Plaque area was measured. Data are means ± SEM from three independent experiments. * $p \leq$
1347 0.05, ** $p \leq 0.01$, *** $p \leq 0.001$, **** $p \leq 0.0001$, Student's *t*-test. Arrowheads show small plaques.
1348 Scale bar= 1mm. B) Tati ΔKu80 parasites were grown in the presence of atovaquone and cKD
1349 TgQCR11 and TgmS35 parasites were grown in the presence of ATc for up to two days. They were
1350 labelled with anti-TgIMC3 (to outline parasites) and *Dolicos biflorus lectin* (DBL) to specifically outline
1351 nascent cyst walls. Scale bar represents 10 µm. DNA was labelled with DAPI. DIC: differential
1352 interference contrast. C) Quantification of DBL-positive vacuoles after 24 hours or 48 hours of culture
1353 of 1) the cKD TgQCR11 and cKD TgmS35 mutants in the presence or absence of ATc 2) the Tati ΔKu80
1354 cell line in the presence or not of 1µM atovaquone. Data are from *n*=3 independent experiments.
1355 Values are mean ±SEM. ** $p \leq 0.01$, *** $p \leq 0.001$, Student's *t*-test. D) The cKD TgQCR11 and cKD
1356 TgmS35 mutants were grown for up to 14 days in the presence of ATc and labelled for tachyzoite
1357 marker SAG1, or early (P18/SAG4) or late (P21) bradyzoite markers. Scale bar represents 10 µm. DNA
1358 was labelled with DAPI. DIC: differential interference contrast.
1359

1360 **Supplemental table legends**
1361
1362 **Table S1. Predicted Toxoplasma homologues of the iron-sulfur cluster synthesis machinery.**
1363 Homology searches were conducted in ToxoBD.org using *Arabidopsis thaliana* proteins as a query.
1364 Putative subcellular localization was obtained from the hyperLOPIT data available on ToxoDB.org, or
1365 by manual annotation. CRISPR fitness score data was obtained from ToxoDB.org.
1366
1367 **Table S2. Predicted Toxoplasma iron-sulfur proteome.** The Toxoplasma predicted whole proteome
1368 was obtained from the ToxoDB.org database and searched for putative iron-sulfur-containing
1369 proteins with the MetalPredator web server (http://metalweb.cerm.unifi.it/tools/metalpredator/).
1370 Putative subcellular localization was obtained from the hyperLOPIT data available on ToxoDB.org, or
1371 by manual annotation. CRISPR fitness score data was obtained from ToxoDB.org.
1372
1373 **Table S3. Proteins with lower or higher expression upon depletion of TgNFS2 as found by label-free**
1374 **quantitative proteomics.** For each protein candidate (with www.ToxoDB.org and www.Uniprot.org
1375 identifier), $\log_2$ of the different ratio were calculated between the mean MaxQuant LFQ values
1376 ('moyLFQ') found for the TgISU1 ('Mito') and TgNFS2 ('Apicoplast') mutants, and the TATi ΔKu80
1377 control ('CTRL'). $-\log_{10}$(pvalue) is also provided. Putative subcellular localization was obtained from
1378 the hyperLOPIT data available on ToxoDB.org, or by manual annotation. CRISPR fitness score and
1379 transcriptomic data for tachyzoites (Tz) and bradyzoites (Bz) were obtained from ToxoDB.org.
1380
1381 **Table S4. Proteins with lower or higher expression upon depletion of TgISU1 as found by label-free**
1382 **quantitative proteomics**. See legend of Table S3. Candidates from the Fe-S proteome (Table S2) that
1383 were found to have a lower expression upon TgISU1 depletion are highlighted in red.
1384
1385 **Table S5. Common proteins with lower or higher expression upon depletion of TgNFS2 or TgISU1,**
1386 **as found by label-free quantitative proteomics.** See legend of Table S3.
1387
1388 **Table S6. Oligonucleotides used in this study.**

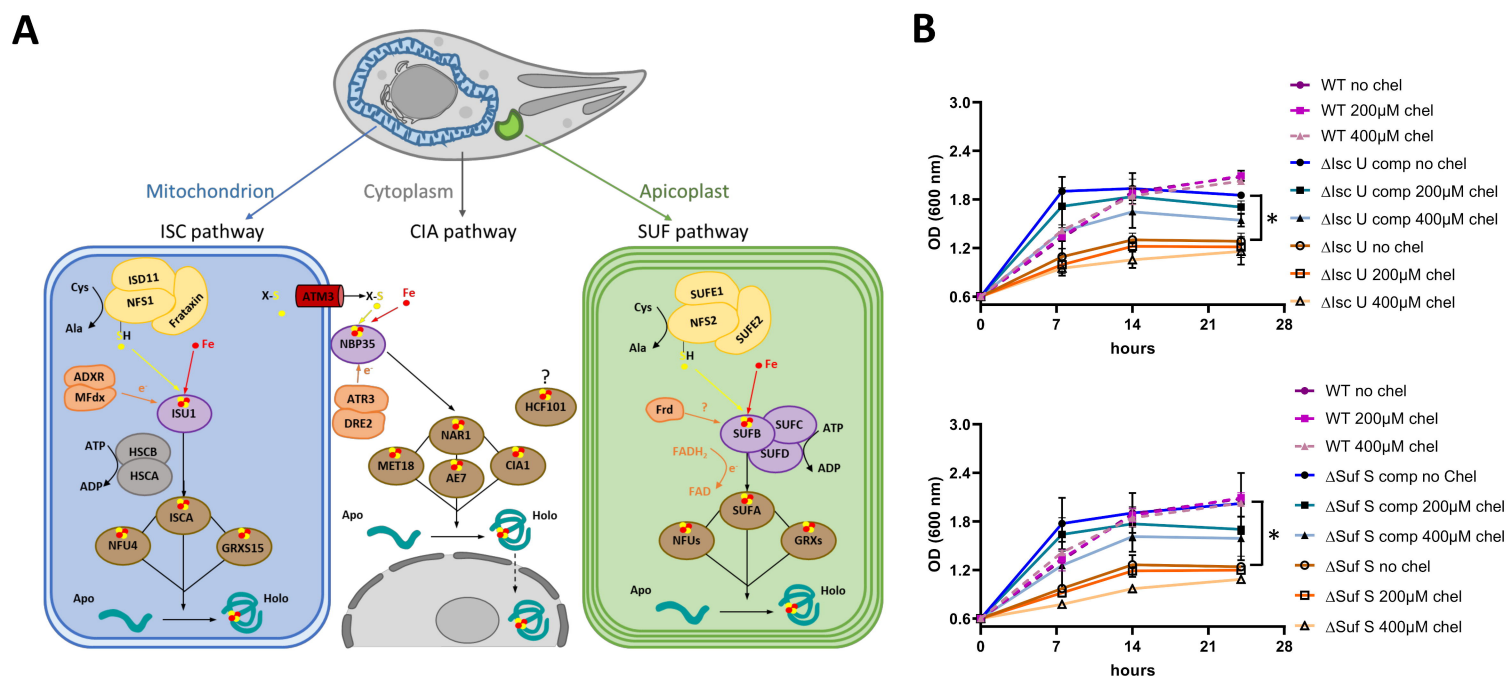
A
Mitochondrion
Cytoplasm
Apicoplast
ISC pathway
CIA pathway
SUF pathway
Cys
Ala
ISD11
NFS1
Frataxin
H
Fe
ADXR
MFdx
e-
ISU1
ATP
ADP
HSCB
HSCA
ISCA
NFU4
GRXS15
Apo
Holo
X-S
ATM3
NBP35
ATR3
DRE2
?
HCF101
NAR1
MET18
AE7
CIA1
SUFE1
NFS2
SUFE2
Frd
SUFB
SUFC
SUFD
FADH2
FAD
SUFA
NFUs
GRXs
B
OD (600 nm)
hours
WT no chel
WT 200µM chel
WT 400µM chel
ΔIsc U comp no chel
ΔIsc U comp 200µM chel
ΔIsc U comp 400µM chel
ΔIsc U no chel
ΔIsc U 200µM chel
ΔIsc U 400µM chel
ΔSuf S comp no Chel
ΔSuf S comp 200µM chel
ΔSuf S comp 400µM chel
ΔSuf S no chel
ΔSuf S 200µM chel
ΔSuf S 400µM chel
*

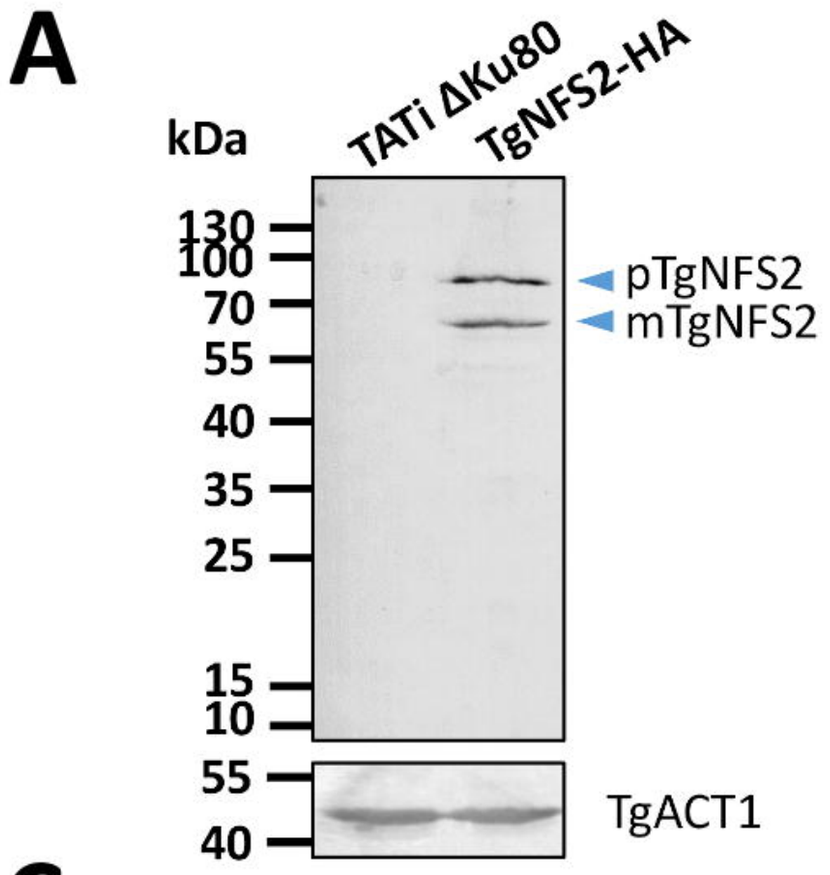
A
kDa
TATi ΔKu80
TgNFS2-HA
130
100
70
55
40
35
25
15
10
pTgNFS2
mTgNFS2
55
40
TgACT1

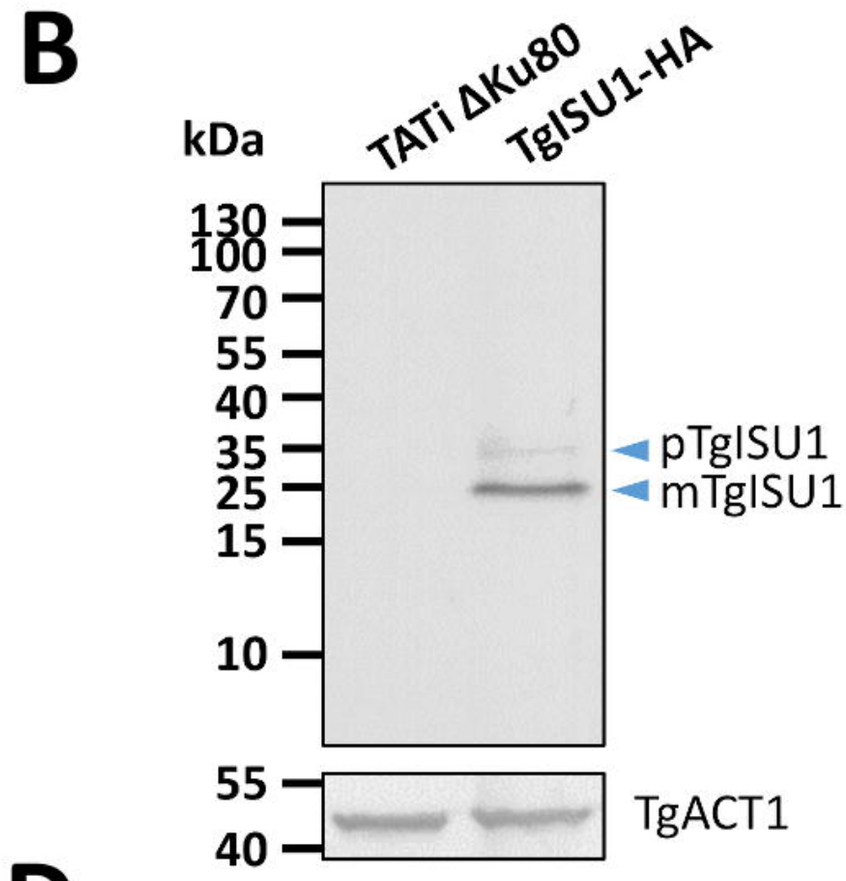
B
kDa
TATi ΔKu80
TgISU1-HA
130
100
70
55
40
35
25
15
10
pTgISU1
mTgISU1
55
40
TgACT1

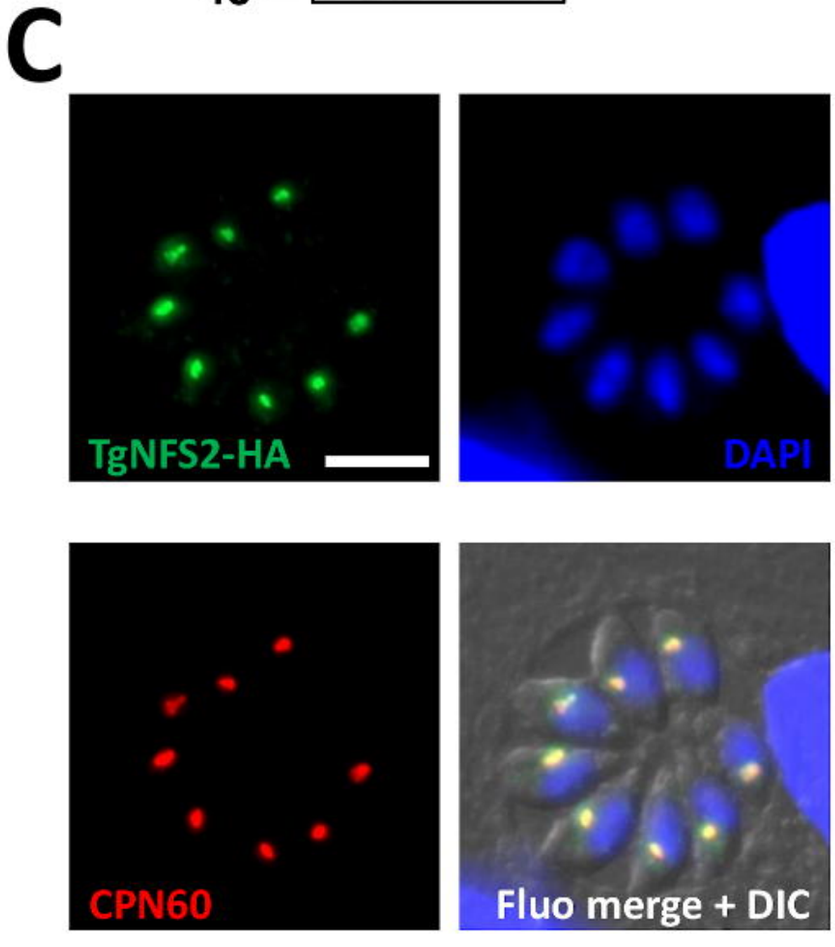
C
TgNFS2-HA
DAPI
CPN60
Fluo merge + DIC

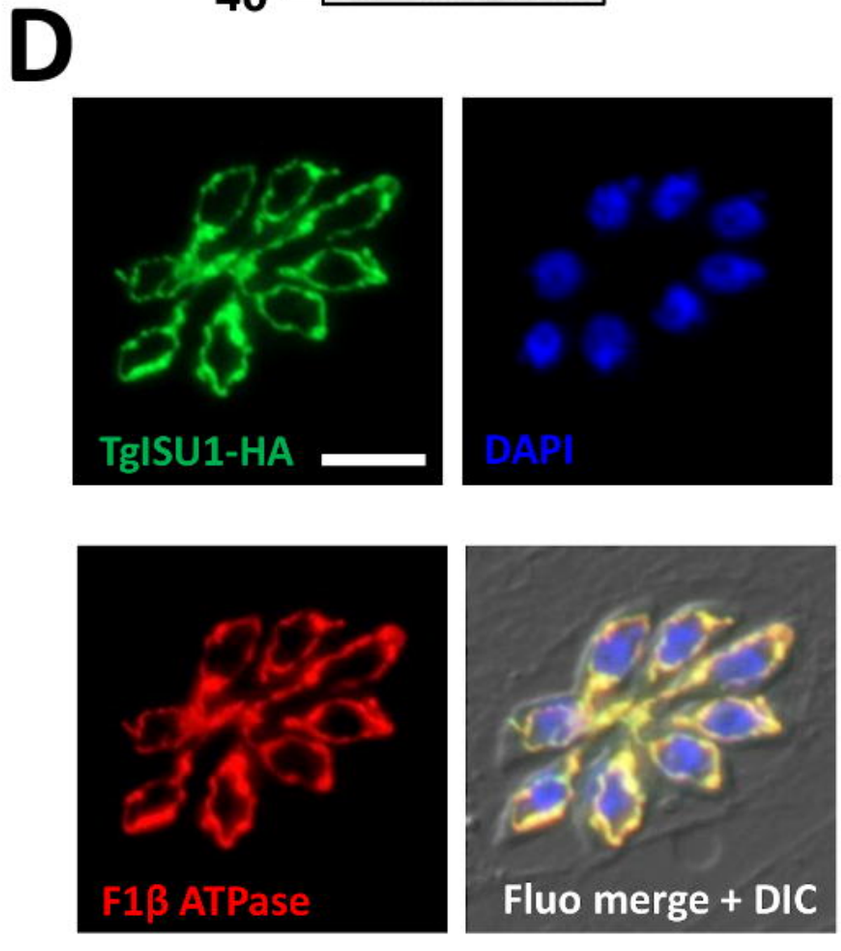
D
TgISU1-HA
DAPI
F1β ATPase
Fluo merge + DIC

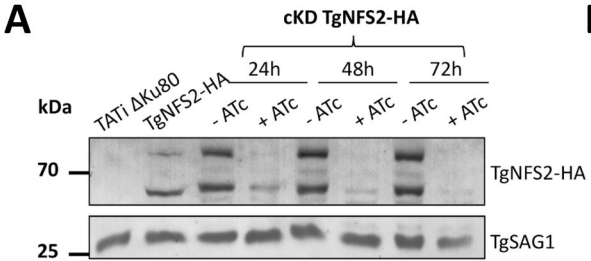
A
cKD TgNFS2-HA
24h
48h
72h
kDa
TATi ΔKu80
TgNFS2-HA
- ATc
+ ATc
- ATc
+ ATc
- ATc
+ ATc
70
25
TgNFS2-HA
TgSAG1

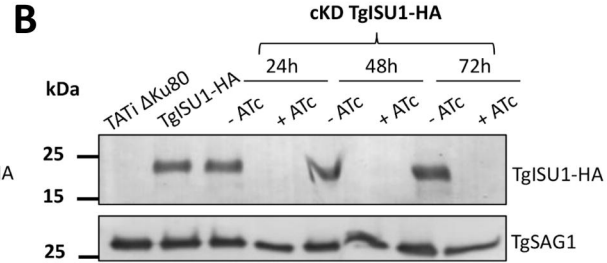
B
cKD TgISU1-HA
24h
48h
72h
kDa
TATi ΔKu80
TgISU1-HA
- ATc
+ ATc
- ATc
+ ATc
- ATc
+ ATc
25
15
25
TgISU1-HA
TgSAG1

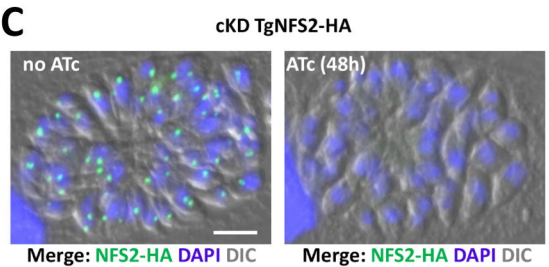
C
cKD TgNFS2-HA
no ATc
ATc (48h)
Merge: NFS2-HA DAPI DIC
Merge: NFS2-HA DAPI DIC

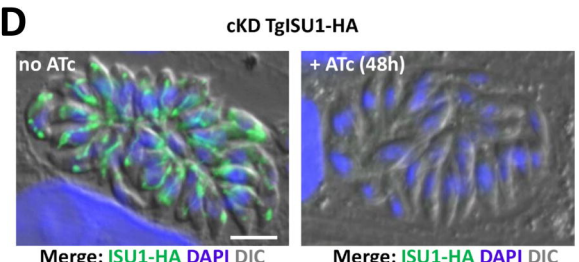
D
cKD TgISU1-HA
no ATc
+ ATc (48h)
Merge: ISU1-HA DAPI DIC
Merge: ISU1-HA DAPI DIC

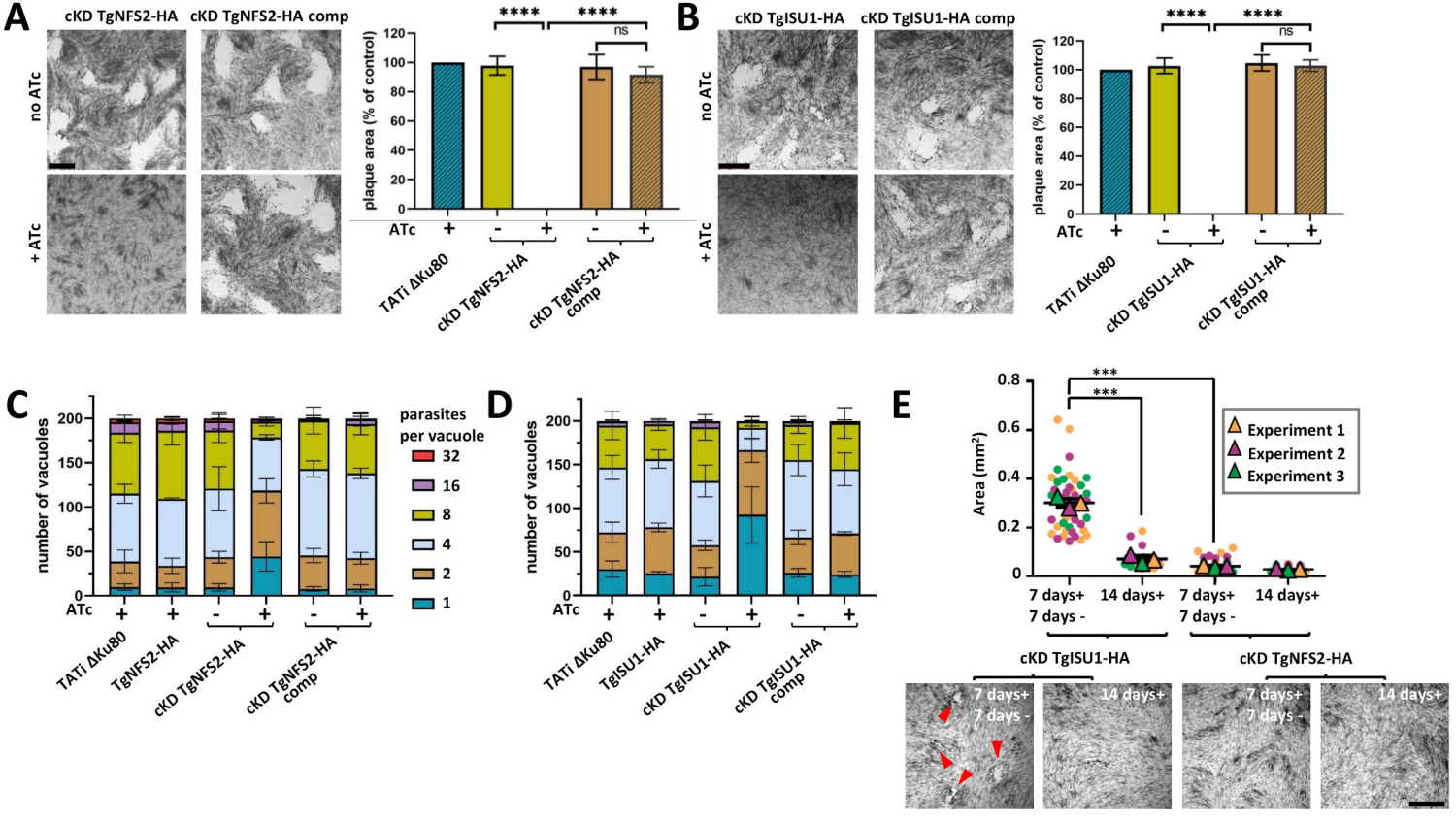
A
cKD TgNFS2-HA
cKD TgNFS2-HA comp
no ATc
+ ATc
plaque area (% of control)
****
****
ns
ATc
TATi ΔKu80
cKD TgNFS2-HA
cKD TgNFS2-HA comp
B
cKD TgISU1-HA
cKD TgISU1-HA comp
cKD TgISU1-HA
cKD TgISU1-HA comp
C
number of vacuoles
parasites per vacuole
32
16
8
4
2
1
TgNFS2-HA
D
TgISU1-HA
E
Area (mm²)
***
***
Experiment 1
Experiment 2
Experiment 3
7 days+ 7 days -
14 days+

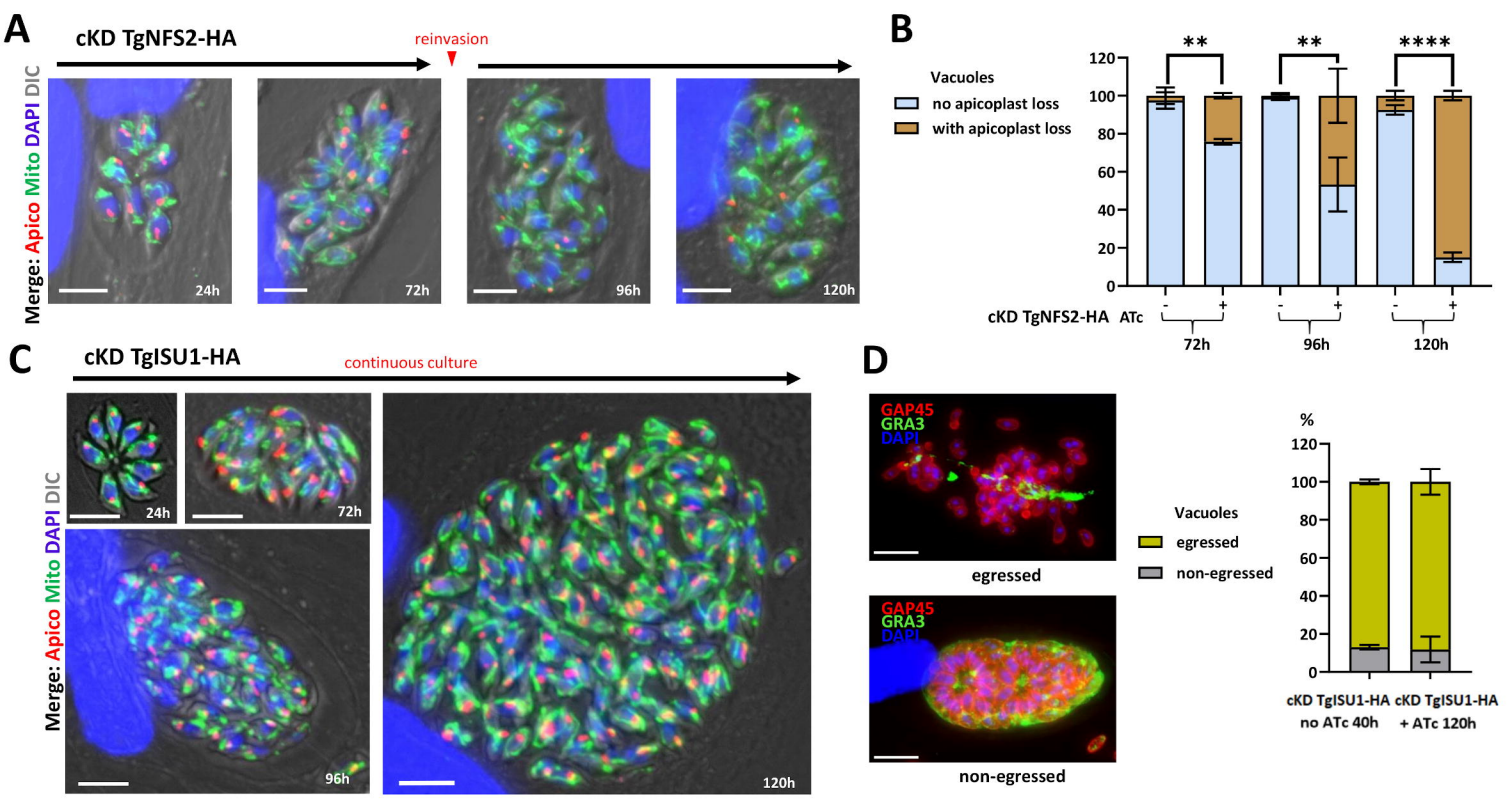
A
cKD TgNFS2-HA
reinvasion
Merge: Apico Mito DAPI DIC
24h
72h
96h
120h
B
Vacuoles
no apicoplast loss
with apicoplast loss
**
**
****
cKD TgNFS2-HA ATc
-
+
72h
96h
120h
C
cKD TgISU1-HA
continuous culture
Merge: Apico Mito DAPI DIC
24h
72h
96h
120h
D
GAP45
GRA3
DAPI
egressed
non-egressed
Vacuoles
egressed
non-egressed
%
cKD TgISU1-HA no ATc 40h
cKD TgISU1-HA + ATc 120h

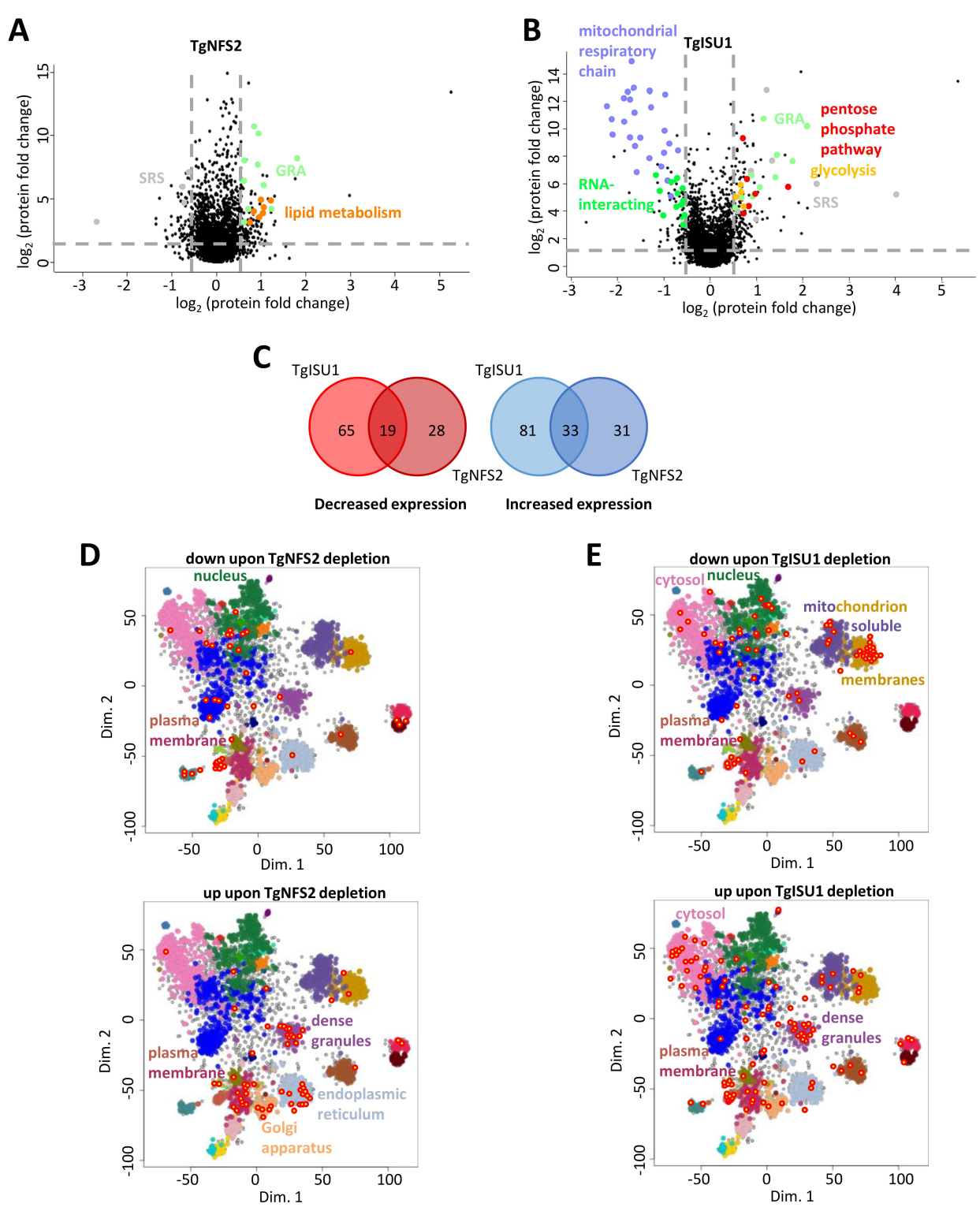
A
TgNFS2
SRS
GRA
lipid metabolism
log2 (protein fold change)
log2 (protein fold change)
B
TgISU1
mitochondrial respiratory chain
GRA
pentose phosphate pathway
glycolysis
RNA-interacting
SRS
log2 (protein fold change)
log2 (protein fold change)
C
TgISU1
65
19
28
TgNFS2
Decreased expression
TgISU1
81
33
31
TgNFS2
Increased expression
D
down upon TgNFS2 depletion
nucleus
plasma membrane
Dim. 2
Dim. 1
up upon TgNFS2 depletion
dense granules
plasma membrane
endoplasmic reticulum
Golgi apparatus
Dim. 2
Dim. 1
E
down upon TgISU1 depletion
cytosol
nucleus
mitochondrion
soluble
membranes
plasma membrane
Dim. 2
Dim. 1
up upon TgISU1 depletion
cytosol
dense granules
plasma membrane
Dim. 2
Dim. 1

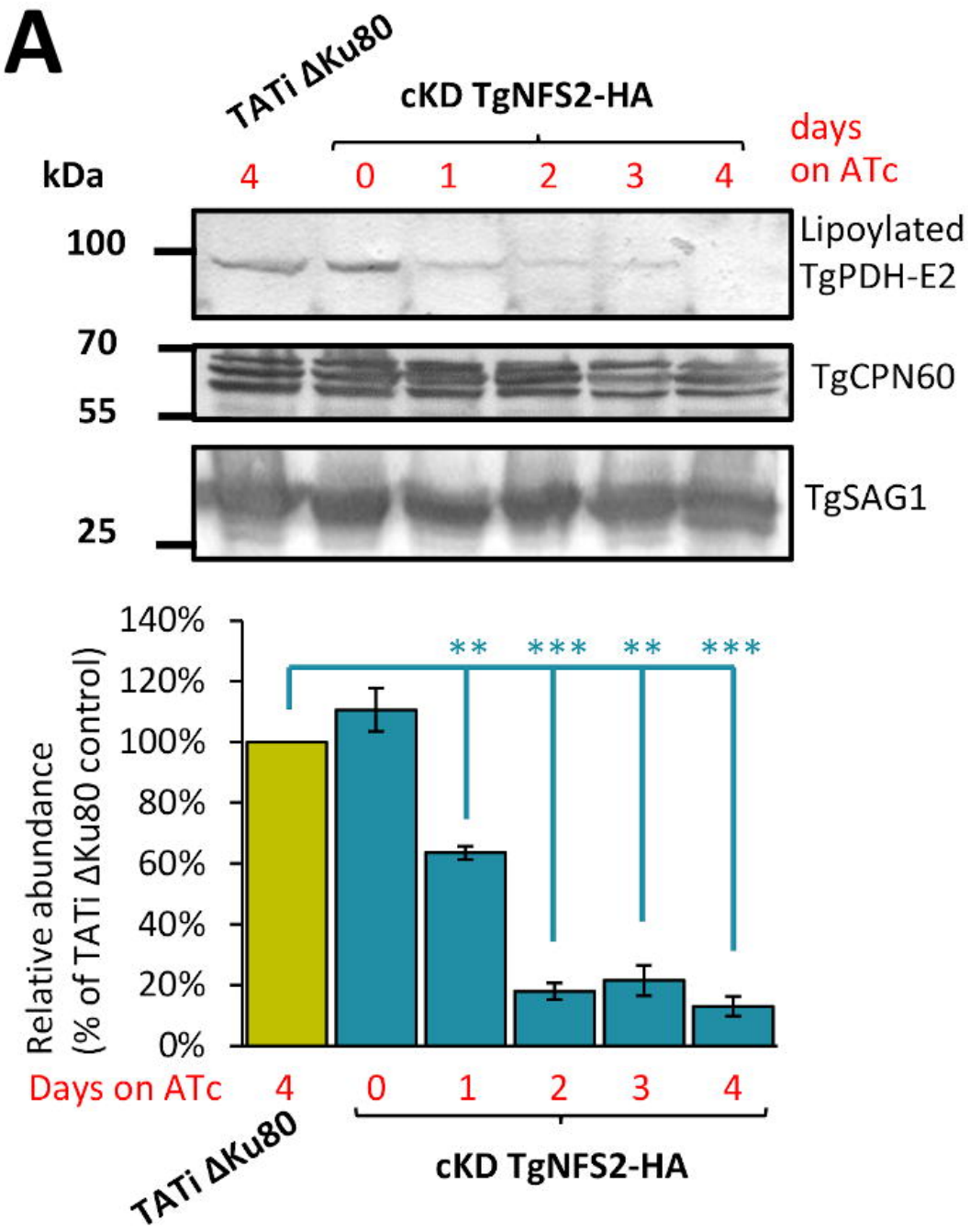
A
TATi ΔKu80
cKD TgNFS2-HA
days on ATc
kDa
4
0
1
2
3
4
100
70
55
25
Lipoylated TgPDH-E2
TgCPN60
TgSAG1
140%
120%
100%
80%
60%
40%
20%
0%
Relative abundance (% of TATi ΔKu80 control)
**
***
**
***
Days on ATc
4
0
1
2
3
4
TATi ΔKu80
cKD TgNFS2-HA

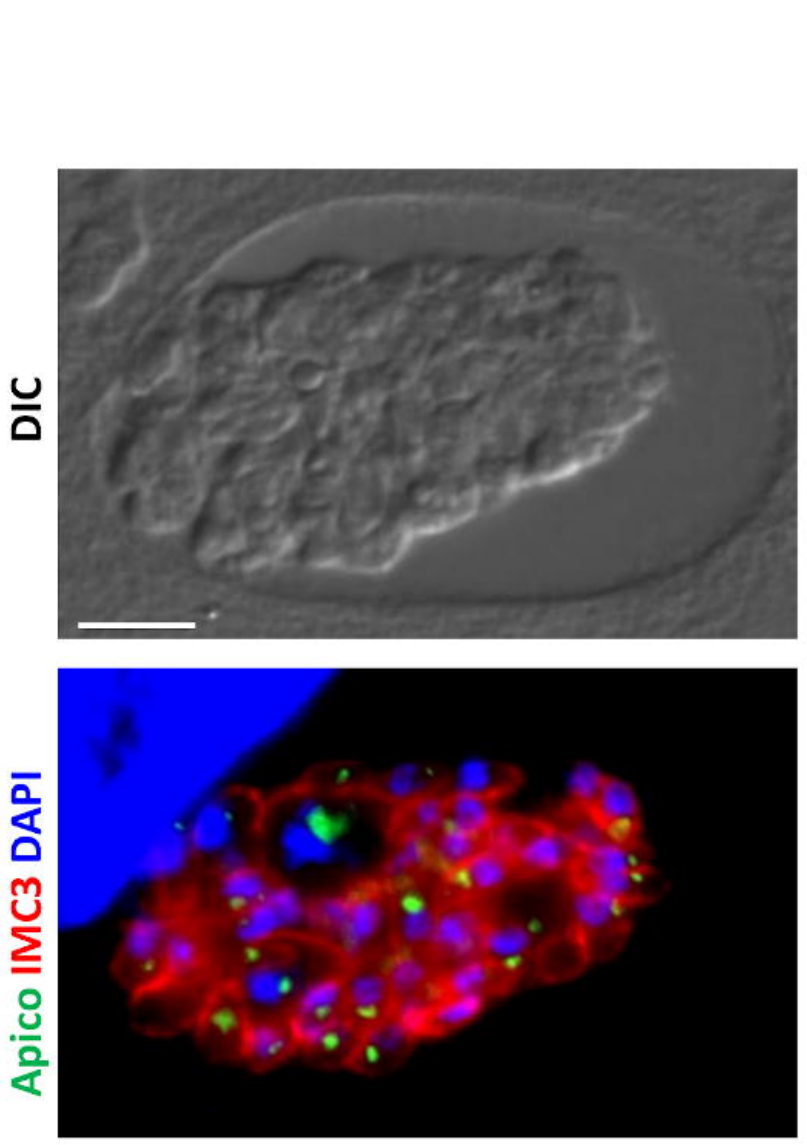
B
DIC
Apico IMC3 DAPI

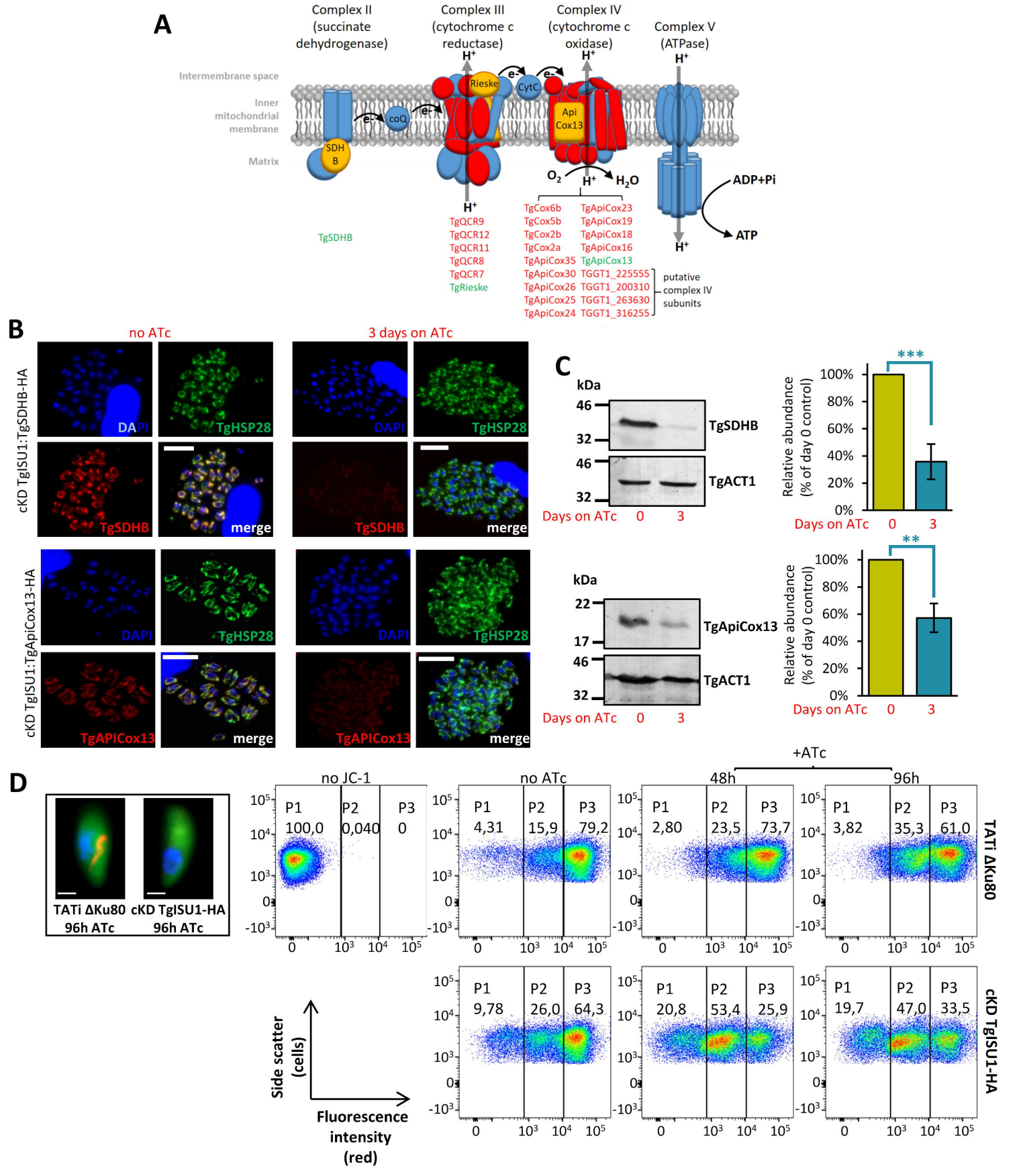
A
Complex II (succinate dehydrogenase)
Complex III (cytochrome c reductase)
Complex IV (cytochrome c oxidase)
Complex V (ATPase)
Intermembrane space
Inner mitochondrial membrane
Matrix
SDH B
coQ
Rieske
CytC
Api Cox13
ADP+Pi
ATP
TgSDHB
TgQCR9
TgQCR12
TgQCR11
TgQCR8
TgQCR7
TgRieske
TgCox6b
TgCox5b
TgCox2b
TgCox2a
TgApiCox35
TgApiCox30
TgApiCox26
TgApiCox25
TgApiCox24
TgApiCox23
TgApiCox19
TgApiCox18
TgApiCox16
TgApiCox13
TGGT1_225555
TGGT1_200310
TGGT1_263630
TGGT1_316255
putative complex IV subunits
B
no ATc
3 days on ATc
cKD TgISU1:TgSDHB-HA
cKD TgISU1:TgApiCox13-HA
DAPI
TgHSP28
TgSDHB
merge
TgAPICox13
C
kDa
TgSDHB
TgACT1
Days on ATc 0 3
Relative abundance (% of day 0 control)
***
**
TgApiCox13
D
TATi ΔKu80 96h ATc
cKD TgISU1-HA 96h ATc
no JC-1
no ATc
+ATc
48h
96h
P1 100,0 P2 0,040 P3 0
P1 4,31 P2 15,9 P3 79,2
P1 2,80 P2 23,5 P3 73,7
P1 3,82 P2 35,3 P3 61,0
P1 9,78 P2 26,0 P3 64,3
P1 20,8 P2 53,4 P3 25,9
P1 19,7 P2 47,0 P3 33,5
TATi ΔKu80
cKD TgISU1-HA
Side scatter (cells)
Fluorescence intensity (red)

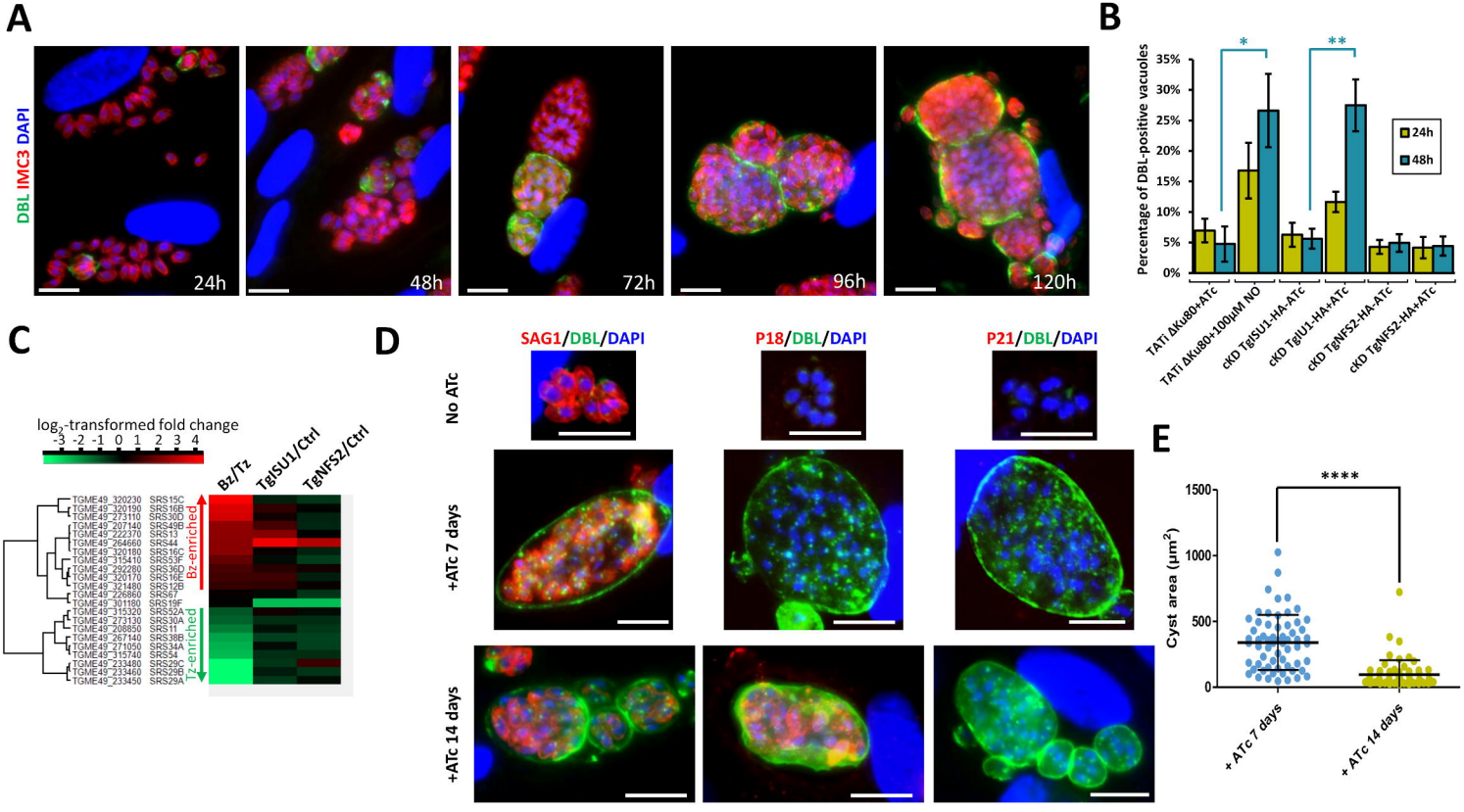
A
DBL IMC3 DAPI
24h
48h
72h
96h
120h
B
Percentage of DBL-positive vacuoles
35%
30%
25%
20%
15%
10%
5%
0%
*
**
24h
48h
TATi ΔKu80+ATc
TATi ΔKu80+100µM NO
cKD TgISU1-HA-ATc
cKD TgIU1-HA+ATc
cKD TgNFS2-HA-ATc
cKD TgNFS2-HA+ATc
C
log2-transformed fold change
-3 -2 -1 0 1 2 3 4
Bz/Tz
TgISU1/Ctrl
TgNFS2/Ctrl
Bz-enriched
Tz-enriched
TGME49_320230 SRS15C
TGME49_320190 SRS16B
TGME49_273110 SRS30D
TGME49_207140 SRS49B
TGME49_222370 SRS13
TGME49_264660 SRS44
TGME49_320180 SRS16C
TGME49_315410 SRS53F
TGME49_292280 SRS36D
TGME49_320170 SRS16E
TGME49_321480 SRS12B
TGME49_226860 SRS67
TGME49_301180 SRS19F
TGME49_315320 SRS52A
TGME49_273130 SRS30A
TGME49_208850 SRS11
TGME49_267140 SRS38B
TGME49_271050 SRS34A
TGME49_315740 SRS54
TGME49_233480 SRS29C
TGME49_233460 SRS29B
TGME49_233450 SRS29A
D
SAG1/DBL/DAPI
P18/DBL/DAPI
P21/DBL/DAPI
No ATc
+ATc 7 days
+ATc 14 days
E
Cyst area (µm²)
1500
1000
500
0
****
+ ATc 7 days
+ ATc 14 days

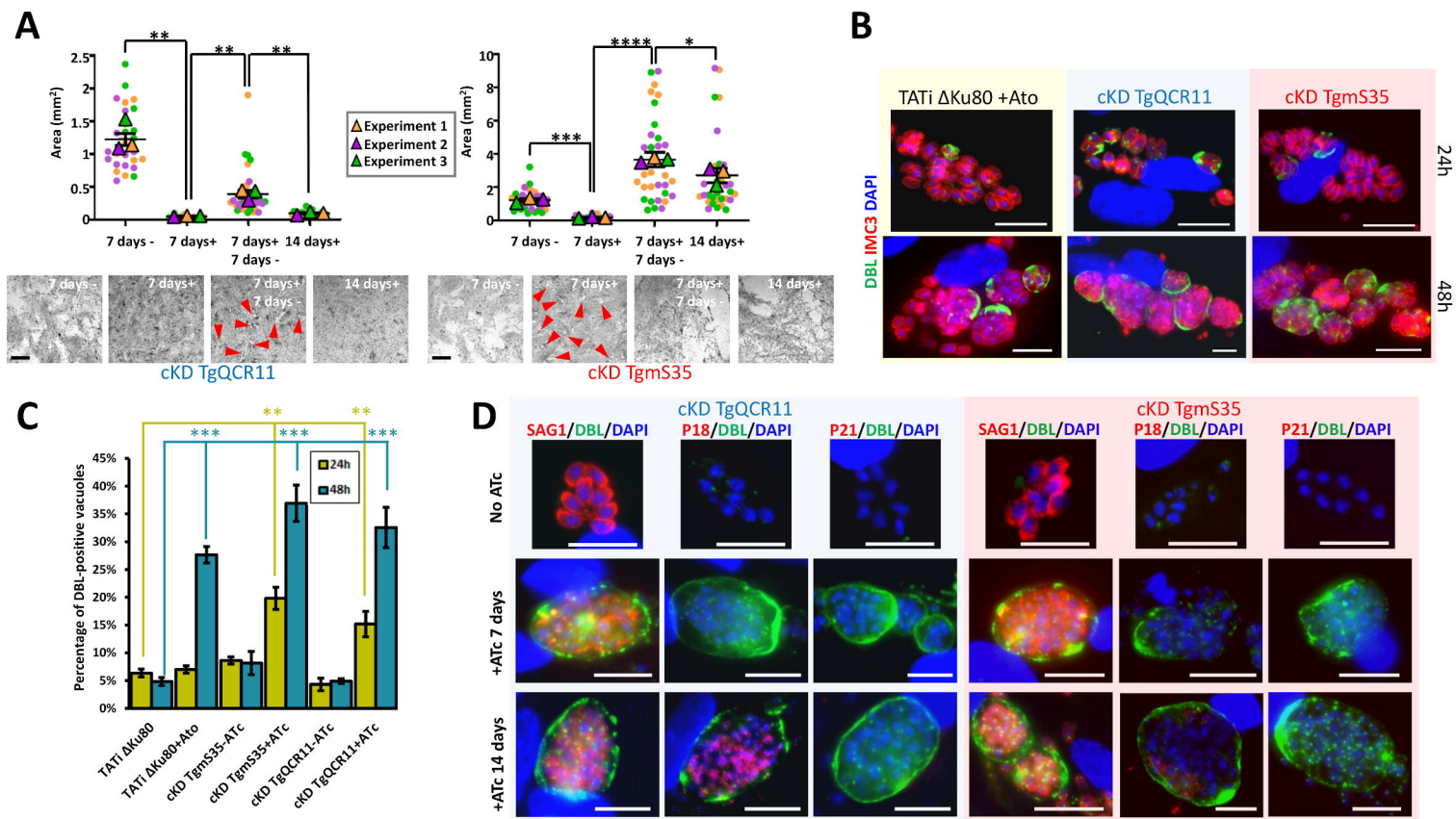
A
Area (mm²)
Experiment 1
Experiment 2
Experiment 3
7 days -
7 days+
7 days+ 7 days -
14 days+
cKD TgQCR11
cKD TgmS35
B
TATi ΔKu80 +Ato
cKD TgQCR11
cKD TgmS35
24h
48h
DBL IMC3 DAPI
C
Percentage of DBL-positive vacuoles
24h
48h
TATi ΔKu80
TATi ΔKu80+Ato
cKD TgmS35-ATc
cKD TgmS35+ATc
cKD TgQCR11-ATc
cKD TgQCR11+ATc
D
cKD TgQCR11
cKD TgmS35
SAG1/DBL/DAPI
P18/DBL/DAPI
P21/DBL/DAPI
No ATc
+ATc 7 days
+ATc 14 days